
Article:
Muir, C.F. orcid.org/0009-0002-6158-9392, Reyes-Aldasoro, C.C., Prajsnar, T.K. et al. (13 more authors) (2025) A subset of neutrophil phagosomes is characterised by pulses of Class I PI3K activity. Disease Models & Mechanisms. ISSN 1754-8403

https://doi.org/10.1242/dmm.052042

A subset of neutrophil phagosomes is characterised by pulses of Class I PI3K activity

Clare F. Muir[1,2,3,*], Constantino Carlos Reyes-Aldasoro[4], Tomasz K. Prajsnar[5], Bartosz J. Michno[5,6], Justyna Cholewa-Waclaw[3], Yin X. Ho[1], Audrey Bernut[7], Catherine A. Loynes[1], Stone Elworthy[1], Kieran A. Bowden[1], Ashley J. Cadby[8], Lynne R. Prince[1], Jason S. King[9], Felix Ellett[10], Alison M. Condliffe[1,*], Stephen A Renshaw[1,*]

[1]Bateson Centre, School of Medicine and Population Health, University of Sheffield, Sheffield, UK
[2]Royal (Dick) School of Veterinary Studies, University of Edinburgh, Edinburgh, UK
[3]Centre of Inflammation, Institute for Regeneration and Repair, University of Edinburgh, Edinburgh, UK
[4]Department of Computer Science, School of Science and Technology, City, University of London, London, UK
[5]Department of Evolutionary Immunology, Institute of Zoology and Biomedical Research, Faculty of Biology, Jagiellonian University, Kraków, Poland
[6]Doctoral School of Exact and Natural Sciences, Jagiellonian University, Kraków, Poland
[7]Laboratory of Pathogens and Host Immunity, Université de Montpellier, Montpellier, France
[8]Department of Physics and Astronomy, University of Sheffield, Sheffield, UK
[9]School of Biosciences, University of Sheffield, Sheffield, UK
[10]Centre for Engineering in Medicine and Surgery, Department of Surgery, Massachusetts General Hospital, Harvard Medical School, Shriners Burns Hospital, Boston, USA

[*]Authors for correspondence: cmuir4@ed.ac.uk; a.m.condliffe@sheffield.ac.uk; s.a.renshaw@sheffield.ac.uk

Keywords: phagocytosis, neutrophils, zebrafish, phosphatidylinositol (3, 4, 5)-trisphosphate, phagosome maturation.

Summary

Class I PI3kinases coordinate the delivery of microbicidal effectors to the phagosome by forming phosphatidylinositol (3, 4, 5)-trisphosphate (PIP3). However, the dynamics of PIP3 in neutrophils during a live bacterial tissue infection are unknown. We have therefore developed an in vivo, live

zebrafish infection model that enables visualisation of dynamic changes in Class 1 PI3kinases (PI3K) signalling on neutrophil phagosomes in real-time. We have identified that on approximately 12% of neutrophil phagosomes PHAkt-eGFP, a reporter for Class 1 PI3K signalling, repeatedly fades and re-recruits in pulsatile bursts. This phenomenon occurred on phagosomes containing live and dead bacteria as well as beads, and was dependent on the activity of the Class 1 PI3K isoform, PI3kinase γ. Detailed imaging suggested that pulsing phagosomes represent neutrophils transiently reopening and reclosing phagosomes, a conclusion supported by observations that a subset of phagosomes in human neutrophils rapidly accumulate dye from the extracellular space. Therefore, we propose that some neutrophil phagosomes remain unsealed and are consequently able to exchange contents with the extracellular environment, with implications for phagosome fate and communication with surrounding cells.

Introduction

Neutrophils are the most abundant white blood cells in the human body and are crucial in the immune system's early defence against bacterial infection. Neutrophils are avid phagocytes, capturing bacteria in membrane-bound vesicles called phagosomes for subsequent execution and digestion. The production of phosphatidylinositol (3, 4, 5)-trisphosphate (PIP3) on phagosome membranes by Class 1 PI3kinases (PI3K) facilitates intra-phagosomal killing of bacteria by coordinating reactive oxygen species (ROS) formation [1,2], degranulation [3,4] and actin dynamics, enabling the phagosome to form and fuse with other organelles [5,6]. However, although PIP3 has been shown to enable phagosome formation around large, inert prey (such as complement component 3 fragment (C3bi)- opsonised zymosan and IgG-opsonised erythrocytes) in neutrophil- and macrophage-like cells [7,8] it is unknown how regulation of PIP3 in space and time controls the maturation of bacterial-containing phagosomes. It is also unknown which PI3K isoform generates

PIP3 on neutrophil phagosomes. The Pleckstrin Homology domain of Akt (PHAkt) recognises PIP3 and also PI(3,4)P2 (a degradation product of PIP3) and has been used extensively to characterise Class 1 PI3K activity in macrophage-like cell lines [6,8–10] and in neutrophil-like cell lines during migration [11] and phagocytosis [7]. Under the control of the neutrophil-specific promoter, *mpx*, PHAkt has also been used to characterise the dynamics of PIP3 and PI(3,4)P2 in migrating zebrafish neutrophils [12]. By developing an *in vivo* infection model using another established transgenic zebrafish neutrophil reporter *Tg(lyz:PHAkt-eGFP)i277* [13], we show that PIP3/PI(3,4)P2 persists on neutrophil phagosomes far longer than *in vitro* macrophage models report and that some PIP3/PI(3,4)P2 positive phagosomes repeatedly reopen and reclose, associated with re-recruitment of the reporter in a pulsatile manner. Pulsing occurs when both live and dead *Staphylococcus aureus* are ingested, as well as *Mycobacterium abscessus* and inert beads, and inhibitor studies suggest this phenomenon is dependent on PI3kinase γ. We suggest that pulsing phagosomes are indicative of repeated cycles of phagosomes reopening and reclosing and that this process follows incomplete sealing of the phagocytic cup.

Results

PHAkt-eGFP recruits to neutrophil phagosomes

To investigate the role of PIP3/PI(3,4)P2 during phagocytosis, we injected *Staphylococcus aureus,* an important pathogen of humans and animals, locally into the somite of the zebrafish neutrophil PIP3/PI(3,4)P2 reporter line, *Tg(lyz:PHAkt-eGFP)i277* [13] (Fig. 1A). Minimal PHAkt-eGFP recruitment was detected during early formation of the phagocytic cup. However, as the phagocytic cup closed, PHAkt-eGFP localised distinctly to sites of cup closure and then, following cup closure, PHAkt-eGFP recruited strongly and uniformly to the entire phagosome membrane (Fig.1B and Movie S1). Following the surge in PHAkt-eGFP recruitment, thin PHAkt-eGFP-positive tubules

extended into the cytoplasm from all phagosomes, and areas of most intense reporter localisation appeared where PHAkt-eGFP-positive tubules recoiled back to join the phagosome membrane. PHAkt-eGFP then gradually diminished on the majority of phagosomes (Fig. 1C-E). However, we observed to our surprise that in a subset of phagosomes, PHAkt-eGFP re-recruited to the phagosome membrane in pulsatile bursts (Movie S2), a phenomenon we then investigated in more detail.

PHAkt-eGFP recruits in pulsatile bursts to neutrophil phagosomes.

A pulse was defined as a transient but intense surge in PHAkt-eGFP recruitment to the phagosome (Fig.2A and B, Movie S2). Repeated pulsing occurred on 12.4% (+/- SD 24.9) of phagosomes within a neutrophil and 35.8% (+/- SD 36.7) of all phagocytic neutrophils had at least one pulsing phagosome. Cycles of PHAkt-eGFP diminishment and then re-recruitment usually started within 10.5mins (+/- 12.49) of phagocytosis and re-recruitment often occurred multiple times (Fig. 2C), typically x4 on each phagosome, but with up to 18 pulses observed on one phagosome. Additionally, we identified that although 17% of neutrophil phagosomes fuse to form larger phagosomes, pulsing phagosomes never fused with other phagosomes and always contained only one bacterium. Some neutrophils phagocytosed more bacteria than others and we wondered whether these hungry phagocytes had more pulsing phagosomes, perhaps reflecting exhaustion of phagocytic capacity [14]. However, we observed the opposite. Pulsing phagosomes occurred more often in less phagocytic neutrophils, with no pulsing phagosomes observed in neutrophils that contained more than 22 bacteria (Spearman's rank correlation=-0.2733, p=0.0415) (Fig.2D).

Pulsatile bursts of PHAkt-eGFP recruitment are neutrophil-initiated.

Having observed that PHAkt-eGFP re-recruits to phagosomes containing live *S.aureus*, we wondered if this phenomenon reflected bacterial manipulation of PIP3/PI(3,4)P2 signalling. To investigate this, *Tg(lyz:PHAkt-eGFP)i277* larvae were injected with heat-killed *S.aureus* (Fig. 3A), hypothesising that pulsing would not be observed if it was due to an active bacterial response to neutrophil attack. However, no significant difference was identified between the percentage of pulsing phagosomes in neutrophils containing live (12.4% +/- SD 24.9) vs dead bacteria (9.3% +/- SD 19.0). Pulsing therefore, does not appear to reflect active manipulation of PIP3/PI(3,4)P2 signalling by *S.aureus*.

To investigate whether phagosomal 'pulsing' is a specific response to *S.aureus*, larvae were injected with a structurally and morphologically distinct prey, *Mycobacterium abscessus* (Fig.3A and B, Movie S3). Pulsatile recruitment of PHAkt-eGFP was again identified and the frequency of pulses was similar to phagosomes containing *S.aureus* (13% +/- SD 26.9) (Fig. 3A), indicating that PHAkt-eGFP re-recruitment occurs irrespective of the species of bacteria engulfed. To distinguish if pulsing is a neutrophil response to phagocytosis of bacteria *vs* non-bacterial prey, larvae were injected with 1µm polystyrene beads (F13083, a size similar to *S.aureus*) (Fig3C: Movie S4). Again, a similar frequency of pulsing was identified (13.36% (+/- SD 19.02) (Fig. 3A). Together, these data suggest that 'pulsing' is a normal neutrophil response to internalisation of potential prey, rather than bacteria attempting to manipulate host signalling.

pH change in pulsing phagosomes differs from non-pulsing phagosomes

We then wished to establish whether pulsing phagosomes mature differently to non-pulsing phagosomes and whether they have the same bactericidal capacity. The pH of human neutrophil phagosomes rises to pH 8.5- 9.0 immediately after particle engulfment and this elevated pH is

maintained for 20–30minutes [15–17]. The rise in pH is attributed to the activity of NADPH oxidase as NADPH inhibition minimises alkalinisation (Fig.S8A-C). NADPH oxidase regulates phagosomal pH through several mechanisms, including consumption of H^+ during H_2O_2 production [18], reducing V-ATPase insertion into the membrane [19], and increasing H^+ leakage through conductive channels [19]. Limited studies have examined how the neutrophil phagosome changes 30mins after phagocytosis. However, studies using fluorescein-stained particles have demonstrated that the neutrophil phagosome gradually acidifies to a pH5.6/6 after 60-120mins [18,20], however, these studies may not be accurate as fluorescein fluorescence dims following exposure to ROS [21]. pHrodo™ fluorescence increases in acidic environments but can still be visualised in pH9 (Fig.S8D) [22]. pHrodo™ staining also does not affect bacterial viability and pathogenicity in the zebrafish infection model (Fig.S9A). Therefore, we choose pHrodo™ as a read-out to compare if the pH of pulsing vs non-pulsing phagosomes differs. In non-pulsing phagosomes, the fluorescence of pHrodo™ stained *S.aureus* was significantly dimmer 10mins after phagocytosis before returning to a similar brightness to pre-phagocytosis (Fig.4A and B). In contrast, within pulsing phagosomes, the fluorescence of pHrodo™ stained *S.aureus* remained similar to that pre-phagocytosis at 10mins and 60mins post-phagocytosis (Fig.4A and B). As pHrodo™ fluorescence dims in alkaline pH (Fig.S8D) [23,24] these findings suggest that pulsing phagosomes alkalinise less than non-pulsing phagosomes shortly after phagocytosis. Additionally, within pulsing phagosomes, there was no significant change in CellROX™ fluorescence (Fig.4C and D). However, within non-pulsing phagosomes, the fluorescence of CellROX™ significantly increased 45mins post phagocytosis (Fig.4C and D). This finding suggests that either there is diminished reactive oxygen species production in pulsing phagosomes and/or that pulsing phagosomes fail to accumulate CellROX™ dye. One potential explanation is that pulsing phagosomes remain open to the external environment.

Pulsatile recruitment of PHAkt-eGFP identifies phagosomes that repeatedly reopen and reclose

During our experiments, we observed neutrophils expelling *S.aureus* from PHAkt-eGFP positive phagosomes (Movie S5). Neutrophils often re-phagocytosed the same bacteria, and in this setting, PHAkt-eGFP once again recruited to the enveloping membranes. During the surge in PHAkt-eGFP recruitment, we also identified that the neck of 9.7% (3/31) phagosomes during a pulsing event formed an elongate tubule, remaining connected to the plasma membrane. Therefore, we considered it possible that such phagosomes had not closed fully or that closure might be imperfect/incomplete. Imaging of this phenomenon was challenging as phagosomes often only opened transiently and via a small pore. However, 3D reconstruction of phagosomes (Fig.5A Movie S6) enabled us to visualise reopening of 19.6% (27/138) of phagosomes during a pulse. On reopening, PHAkt-eGFP recruitment rapidly dropped, with the bacteria usually remaining within the newly opened phagocytic cup, before the phagosome resealed (Fig.5A and Movie S6). To confirm that pulsing phagosomes re-open, actin and PHAkt dynamics were assessed in parallel using larvae of *Tg(lyz:PHAkt:GFP)i277* x *Tg(mpx:Lifeact-Ruby)SH608*. This showed that cortical actin filaments separated as pulsing phagosomes approached the neutrophil surface and remained on either side of the phagosome as the phagocytic cup opened to release the prey. After the phagocytic cup reformed and recaptured prey, cortical actin filaments then propelled the phagosome inwards once again (Fig.S10). This confirmed that PHAkt-eGFP decreases when phagosomes re-open and release bacteria, and that PHAkt re-recruits to phagosomes when they recapture expelled bacteria (pulsing). We also observed a distinct increase in the fluorescence of pHrodo-stained *S.aureus* when bacteria were released into the tissue, a less alkaline environment than the early neutrophil phagosome [16,19] (Fig.5B). The fluorescence of pHrodo™-stained *S.aureus* then decreased as the bacteria was rephagocytosed, as is expected as neutrophil phagosomes rapidly alkalinise during phagocytosis [16,25] (Fig.5B). In 5.1% (7/138) 'pulses', bacteria were fully released from the phagocytic cup but remained close to the neutrophil

surface before being recaptured. 94% (29/31) of bacteria from 'pulsing' phagosomes were successfully recaptured by the same neutrophil. 3% (1/31) bacteria were released and then re-phagocytosed by a non-fluorescent phagocytic cell (presumed macrophage), and 3% (1/31) bacteria were shuttled into another neutrophil [26].

Having observed that some pulsing phagosomes reopen, we wished to determine whether this phenomenon followed a failure of the phagosome to seal or whether this followed an active exocytosis event. To achieve this, we allowed human neutrophils to phagocytose *S.aureus* for 30 minutes and then added the cell membrane impermeable dye, Lucifer yellow. 20.1% (+/- SD 2.9) of phagosomes containing live *S.aureus* rapidly accumulated Lucifer yellow fluorescence (Fig 5C and D). Given that simultaneous exocytosis events would be unlikely to occur for this number of phagosomes [27], we propose that these leaky phagosomes remain unsealed. Additionally, the fluorescence of pHrodo™ stained *S.aureus* was less bright within phagosomes that accumulated Lucifer yellow (Fig.5E), suggesting that unsealed phagosomes may acidify less than those that remain sealed.

Pulses of PHAkt-eGFP are abolished by PI3K γ inhibition

During imaging, we identified that PHAkt-eGFP uniformly increases on the phagosome membrane as the phagocytic cup closes and that there is a second increase in PHAkt-eGFP recruitment at the neck of the phagosome, prior to sealing. We next aimed to identify the Class 1 PI3Kinase enzyme, which drives dynamic PIP3 production on neutrophil phagosomes [28]. The three tyrosine kinase-linked Class1A PI3kinase isoforms are α, β, and δ, and the sole G-protein activated Class1B PI3kinase isoform is PI3K γ [28]. Neutrophils express abundant PI3kinases γ and δ [28] and, in zebrafish, inhibition of PI3kinase γ completely abolishes the migration of neutrophils to an injured tail fin [12].

Although unexplored in a zebrafish infection model, PI3kinase δ inhibition has been reported to reduce the migration of human neutrophils *in vitro* [29] and also reduces neutrophil migration towards a TNFα injection site in a mouse. This makes it difficult to assess whether neutrophils from transgenic fish lacking PI3kinase γ or δ phagocytose prey *in vivo*, as such neutrophils will not migrate to the infection site. To assess the role of PI3kinases γ and δ in phagocytosis, neutrophils were therefore allowed to migrate to the infection site for 60mins and then zebrafish were exposed to class 1 PI3kinase inhibitors. Based on our published previous work using these inhibitors in the zebrafish models [30], we incubated larvae for 30mins with 100μm of the PI3kinase δ inhibitor, CAL-101(IC50 = 2.5nM, EC50=8nM [31]) before immediately commencing imaging. The relatively high inhibitor concentration reflects the need for penetration into the tissues. Although CAL-101 decreased both the total number of neutrophils and the number of phagocytic neutrophils at an infection site (Fig.S11A and B), in both control zebrafish and zebrafish exposed to CAL-101, pulsatile bursts of PHAkt-eGFP recruitment occurred on neutrophil phagosomes (Fig.6A-C). This data suggests that PI3kinase δ does not mediate the pulsatile recruitment of PHAkt-eGFP to neutrophil phagosomes.

We titrated the dose of PI3K γ inhibitor AS605240 (IC50=8nM[32], EC50= 117nM[33]) to identify that a delayed 30mins incubation with 1μm of this compound significantly decreased the % of PHAkt-eGFP positive phagosomes, but not the number of neutrophils recruited to the infection site nor the number of bacteria internalised per neutrophil (Fig.6D-F). This suggested to us that neutrophils recruited to the infection site and phagocytosed bacteria in the 60mins before the PI3K γ inhibitor was applied. However, the subsequent application of AS605240 then reduced the production of PIP3/PI(3,4)P2 on neutrophil phagosomes (Fig.6G: Movie S7). Close examination of time-lapses of AS605240-treated larvae showed that although some PHAkt-eGFP recruited to neutrophils as they initiated phagocytosis, the later larger surges of PHAkt-eGFP recruitment, firstly to the fully formed phagocytic cup and secondly, to the neck of the phagosome during closure, did not occur. In the

absence of PHAkt-eGFP recruitment to phagosomes, the partially phagocytosed bacteria were released back into the tissue. Occasionally, neutrophils attempted to re-phagocytose the bacteria but again, visible re-recruitment of PHAkt-eGFP ('pulsing') was absent (Fig.6A, B and G: Movie S7). We, therefore, concluded that PI3kinase γ enables phagocytosis. We propose that without functional PI3kinase γ activity, initiated neutrophil phagosomes fail to close effectively, and prey is subsequently released into the tissue but not re-captured.

Discussion

Using an *in vivo* model of Class 1 PI3K signalling, we have identified an intriguing new phenomenon by which neutrophils repeatedly reopen and reclose a significant proportion of phagosomes. This phenomenon occurs following phagocytosis of structurally and morphologically distinct bacteria, as well as inert beads.

In the majority of phagosomes, we were unable to visualise continuity between the phagosome and cell membrane using *in vivo* imaging techniques. It is therefore possible that pulsing phagosomes may have fully sealed and then re-fused with the plasma membrane to release prey (non-lytic exocytosis)[34–36]. However, using human neutrophils we demonstrate that a subset of formed neutrophil phagosomes rapidly accumulate dye from the extracellular space. Given that simultaneous exocytosis events would be unlikely to occur for this number of phagosomes [27], we suggest that these 'leaky' phagosomes remain connected to the extracellular space. Unsealed phagosomes may repeatedly reopen and close, and thus generate pulses of class 1 PI3 activity as the neutrophil attempts to recapture partially released bacteria.

We speculate that unsealed phagosomes may aid the release of partially degraded material into the extracellular space and that this may facilitate exchange between the phagosome and the infected

tissue. A process, termed 'eructophagy', occurs in primary human and murine macrophages [27] and describes the release of partially digested bacterial DNA into the extracellular space that then activates pro-inflammatory signalling pathways in neighbouring cells [27]. Eructophagy occurs in approximately 10% of phagolysosomes over a 3-hour period and is stimulated by inflammation and nutrient depletion. However, eructophagy only occurs 2-10 hours after phagocytosis and in phagosomes that have acidified and fused with lysosomes[27] (i.e. after phagosome maturation). In contrast, we propose that shortly after phagocytosis, a minority of nascent neutrophil phagosomes remain unsealed and connected to the extracellular environment.

We identified that recruitment of PHAkt to neutrophil phagosomes is dependent at least in part on PI3kinase γ activity. This suggests that PI3kinase γ, in addition to playing a key role in enabling neutrophil migration [11], might enable bacteria-containing phagosomes to seal. Supporting our findings, Quinn *et al.,* 2021 identified that Class 1PI3 kinases, which include PI3kinase γ, enable macropinosomes to seal [37] and potentially similar mechanisms may underpin phagocytosis of bacteria. There are two regulatory subunits for PI3kinase γ, namely p84 and p101, each of which coordinates different neutrophil responses[38,39]. Future work may determine which PI3kinase γ regulator(s) enable PIP3 production on bacterial-containing phagosomes to facilitate closure. This is important as it may allow selective therapeutic targeting of neutrophil function. For example, although there are currently no p84/p101 inhibitors, selective nanobodies have recently been developed that can selectively target the different PI3kinase γ inhibitory complexes [40].

Additionally, in contrast to neutrophils phagocytosing yeast *in vitro* [7], the intensity of PHAkt-eGFP only slightly increased as neutrophil membranes wrapped around bacteria. Instead, PHAkt-eGFP intensity increased firstly as opposing membranes appeared to touch and secondly, with greatest intensity, on the entire phagosome as the phagosome appeared to be internalised. This may reflect

differences in how PI3kinases coordinate phagocytosis in neutrophils vs macrophages, zebrafish vs human cells and/or the phagocytic target, e.g. Ig opsonised beads vs bacteria.

In conclusion, we have developed an *in vivo* model to image Class1 PI3K signalling in real-time during a bacterial infection. This model has enabled us to identify that PI3kinase γ produces the majority of PIP3/PI(3,4)P2 on bacterial phagosomes and that the majority of PI3kinase γ activity occurs after bacteria are internalised by the neutrophil. Additionally, pulses of class 1 PI3K activity occur when neutrophils repeatedly reopen and reclose phagosomes and a slightly higher proportion of human neutrophil phagosomes rapidly accumulate dye when it is added to the extracellular space. Our quantification of the % of unsealed phagosomes in zebrafish may be an underestimate as we could only identify phagosome reopening by a pulse of class 1 PI3 activity, rather than, the more accurate accumulation of dye from the extracellular space.

This intriguing finding suggests that a subset of neutrophil phagosomes remain open and we speculate that this may be a normal part of neutrophil phagosome maturation to aid exchange between the intra and extracellular environment.

Methods

RESOURCE AVAILABILITY

Lead contact

Further information and requests for resources and reagents should be directed to and will be fulfilled by the lead contact, Clare Muir (cmuir4@ed.ac.uk).

Materials availability

Data and code availability

Microscopy data reported in this paper will be shared by the lead contact upon request.

All original code has been deposited in the GitHub repository https://github.com/reyesaldasoro/RingFluorescence and is publicly available as of the date of publication. DOIs are listed in the key resources table.

Any additional information required to reanalyse the data reported in this paper is available from the lead contact upon request.

EXPERIMENTAL MODEL DETAILS

Animal work was carried out according to guidelines and legislation set out in UK law in the Animals (Scientific Procedures) Act 1986, under Project License PP7684817. Ethical approval was granted by the University of Sheffield Local Ethical Review Panel. Adult Zebrafish and larvae were maintained in the Bateson Centre aquaria at the University of Sheffield and maintained according to standard protocols [43]. The aquarium is a continuous re-circulating closed system with a light-dark cycle of 14/10 hours respectively and a temperature of 28°C. Existing lines were London wild-type (LWT), *Nacre* and *Tg(lyz:PHAkt-eGFP)i277*. Larvae were maintained in E3 (5 mM NaCl, 0.17 mM KCl, 0.33 mM CaCl2, 0.33 mM MgSO4) plus methylene blue (Sigma-Aldrich, 50,484) at 28°C until 3dpf.

METHOD DETAILS

Bacterial strain and growth conditions

S.aureus strain USA 300 [41] and *M. abscessus* strain CIP104536T morphotype smooth was were used for all experiments [42]. Overnight cultures of *S.aureus* were started from single colonies and grown in 10mL brain heart infusion medium (Sigma, 53286) overnight at 37°C, shaking at 250rpm. In the morning, cultures were diluted 1:100 and grown for 2.5hours. Cultures were pelleted at 4500g for 15mins at 4°C (Sigma, USA 3-16KL, 11240 x 13145 rotor) and resuspended in PBS (Oxoid, BR0014 G) to 1500cfu/nL. For specific experiments, *S.aureus* was killed by heating in an 80^{o}C water bath for 20mins. *M. abscessus* cultures were grown and prepared for infection challenges (150cfu/nl) as previously described [42].

pHrodo™ staining of bacteria

200µL of PBS/bacterial suspension was then added to 1µL of pHrodo™ Red (Thermo Fisher Scientific, P36600 or P35369), incubated at 37 °C, 100 rpm for 30mins. Stained bacteria were then washed with 1mL of PBS, 1mL 30 mM Tris pH 8.5 and final wash of 1mL of PBS before resuspending in PBS for injection.

Zebrafish injections

Zebrafish larvae were injected using borosilicate glass needles (World Precision, Instruments, USA, TW100-4) and a pneumatic PicoPump (PV820 World Precision Instruments, USA). Borosilicate glass needles were prepared using a horizontal micropipette puller (P-1000 Sutter Flaming/Brown™) and subsequently loaded with 7µl of inoculum prepared as above using an Eppendorf ™ Microloader™ Pipette Tip. The needle was orientated into the desired position using a

micromanipulator (World Precision Instruments, USA) and a stereomicroscope (Nikon microscope SMZ 745). Fine tweezers were then used to break the needle tip and the inoculum drop was then calibrated to 1nL by using a graticule (Pyser Optics) coated with mineral oil. The 18^{th}-20^{th} dorsal somite of day-3 zebrafish larvae was then injected and the infection site was time-lapsed from 30 mpi.

Microscopy

Larvae were mounted in a 1% low-melting-point agarose solution (Affymetrix, 32,830) containing 0.168 mg/mL tricaine. Agarose was covered with 500µl of clear E3 solution. Imaging was performed from 30min until 3hours post-injury using a 40x oil objective (UplanSApo 40x oil [NA 1.3]) on an UltraVIEWVoX spinning disk confocal laser imaging system (Perkin Elmer) with a Hamamatsu C9100-50 EM-CCD camera. Fluorescence for eGFP and pHrodo™ Green was acquired using an excitation wavelength of 488nm, emission was detected at 510nm. Fluorescence for pHrodo™ Red and crimson was acquired using 525nm emission and detected at 640nm. 25-40µm z stacks were captured with a step interval of 1.5µm.

Image Analysis

Images were processed using Fiji and Matlab® (Mathworks™, Natick, USA). Phagosomes were analysed for a mean of 72mins (6.4-191.7mins +/- SD 56.7). Phagosomes were tracked using TrackMate [47]. On average, phagosomes were analysed for 72 mins (6.4-191.7mins +/- SD 56.7). The position of the phagosomes was obtained using the tracking plug-in TrackMate [48] and all subsequent analysis was performed in Matlab. The volumetric analysis of the phagosomes was performed with an intensity based-segmentation on each of the 3D volumes. All channels were smoothed in 3D with a box kernel of size [3x3] and then intensity levels were used to perform an intensity-based

segmentation. For the green channel two intensity levels were employed, one low that corresponded to the whole neutrophil and one high that corresponded to the phagosome. The red channel only required one level that corresponded to the bacteria. The volumes of the bacteria inside and outside the neutrophil were measured and the ratio of inside and outside was calculated as well as the average intensities for all frames. To display the volumes, isosurfaces were calculated and displayed as meshes (Fig. 3A). To calculate the intensities of the phagosomes over time, the positions were recorded as previously mentioned and then the intensities of all pixels within a ring of radius of 6 pixels were extracted. The average intensity inside the ring was calculated as well as the intensities as a function of the angle, in particular 21 directions were calculated, to visualise if the intensity was uniform around the ring or if it was higher in one side than in the other. For this study 9 phagosomes in four different datasets were analysed. Each track consisted of a 2D dataset of dimensions [number of time frames x 21] where the 21 corresponded to the angles of the ring. The intensity values were low pass filtered to smooth the results (Fig. 1A). Finally, the intensity values of the 9 tracks were averaged to calculate mean and standard deviation. First, intensities were normalised by subtracting the minimum value of the track and then dividing by the maximum so that the range of values was within 0 and 1. Next, the tracks were shifted in time so that all the start of all tracks coincided in a new time 0 and could be compared. Then mean and standard deviation per time frame were calculated (Fig.1A). The code is publicly available through GitHub in the repository: https://github.com/reyesaldasoro/RingFluorescence.

Image analysis of human neutrophils was performed using Harmony software (Revvity) by segmenting pHrodo™ Red-stained bacteria inside neutrophils and then measuring the mean intensity of Lucifer Yellow within the mask. Threshold was applied to determine Lucifer Yellow positive and negative fraction of bacteria-filled phagosomes.

Preparation of beads

50µLs of a 2% solution of 1µm crimson beads (Thermo Fisher Scientific, F8816) was diluted, washed and then resuspended in 500µLs of PBS. 1nL of this suspension was then injected into the 18th-20th dorsal somite of day-3 zebrafish larvae.

Preparation of neutrophil actin reporter

Tg(mpx:Lifeact-Ruby)sh608 was made by injecting single-cell larvae with the destination plasmid, *Tol2-mpx:Lifeact-Ruby* (a gift from Anna Huttenlocher) with the tol2 transposase RNA generated as previously described [43].

Injection with CellROX™ reagent

1µL of CellROX™ Deep Red Reagent was added to 50µLs of 1500cfu/nL *S.aureus* culture.

Preparation of human neutrophils

Human neutrophils were isolated by Plasma-Percoll density gradient centrifugation from whole blood of healthy donors as previously described [49]. The study was carried out with written informed consent obtained from each donor. The ethical approval was obtained from the Edinburgh Medical School Research Ethics Committee (21-EMREC-41). Freshly isolated neutrophils were resuspended at $0.3x10^6$ cells/mL in phenol red-free Roswell Park Memorial Institute (RPMI) 1640 media (Thermo Fisher, Waltham, MA), supplemented with 10% (w/v) heat-inactivated fetal bovine serum (FBS, PromoCell, Heidelberg, Germany) and 25mM HEPES buffer solution (Sigma Aldrich, Gillingham, Dorset). Neutrophils were cultured in a 96-well #1.5, ibiTreat polymer treated plate (89606, Ibidi, Martinsried, Germany). Freshly isolated neutrophils ($9x10^4$ cells) were incubated at 37°C for 30mins. pHrodo™ Red stained *S.aureus* (JE2) was then added and the plate was spun at 100g for 1min to synchronise phagocytosis before incubating for 15mins at 37°C. Neutrophils were then stained with

10µg/mL of CellMask™ Deep Red plasma membrane stain (C10046, Invitrogen, Carlsbad, CA) before incubating for another 10mins at 37°C. Neutrophils were then timelapsed for 5mins before the addition of 50µg/mL of Lucifer Yellow (L453, ThermoFisher). A 60mins timelapsed of the same neutrophils was commenced immediately after the addition of Lucifer Yellow.

Microscopy of human neutrophils

Live imaging of human neutrophils were performed on an Opera Phenix (Perkin Elmer, Waltham, United States), using excitation wavelength of 425, 561 and 647nm. Neutrophils were maintained at 37°C using the inbuilt incubator of the Opera Phenix.

Drug treatment of zebrafish

Day 3 zebrafish larvae were immersed in 1µm AS605240 and 100 µm CAL-101 (Selleckchem, Houston, USA) in 1% DMSO in E3 medium. Larvae were incubated in inhibitors at 28°C for 30mins before imaging. Controls were similarly immersed in 1% DMSO in E3.

DPI inhibition and ROS imaging within *S. aureus* infected zebrafish neutrophils

DMSO- and DPI-treated (100 µm) neutrophil-repleted (*irf8* knockdown) [44] ABTL larvae at 48 hpf were co-injected with 1500 CFU of pHrodo™ Red-labelled JE2 and 10mM DCFDA (2′,7′-dichlorofluorescin diacetate, Sigma, 287810). At 1 hpi, larvae were imaged using a Zeiss LSM 900 with a 20x objective, NA 0.8. The 488 and 561 nm laser lines were used. pHrodo™ Red and DCF fluorescence intensity was quantified using an ImageJ custom script called Fish Analysis v5 [45]. All bacterial clusters were identified based on their pHrodo™ Red fluorescence and non-phagocytosed bacteria were disregarded. The fluorescence intensity of the DCF surrounding the phagocytosed bacteria (0.5µm radius) was quantified. Subsequently, we calculated the ratio of the DCF

fluorescence surrounding the bacteria divided by the signal from non-infected phagocytes to normalize the results by the baseline ROS signal in neutrophils of both DMSO and DPI groups.

Zebrafish Survival Curves

1900 CFU of pHrodo™ Red labelled and unstained JE2 were injected into the circulation of 48hpf ATBL larvae as described previously [44].

Quantification and statistical analysis

Prism software (GraphPad, Inc.) was used to perform statistical analysis. Precision measures, n values and statistical tests used are indicated in all figure legends. P = <0.05 was used to determine significance.

Acknowledgements

We would like to acknowledge the research support teams at the University of Sheffield. We thank the aquarium staff for the breeding and maintenance of our zebrafish strains as well as the Wolfson Light Microscopy Facility and the Institute for Regeneration and Repair Imaging facility. We would also like to thank Professor Sarah Walmsley and Professor David Dockrell for their ideas and support of this project, the blood donors and CIR blood user database. We would also like to thank Professor Anna Huttenlocher for her gift of the Tol2-mpx:Lifeact-Ruby plasmid. This work was supported by the Wellcome Trust (R/151624) and the Biotechnology and Biological Sciences Research Council (B/V019368/1). BJM and TKP were supported by National Science Centre of Poland within Sonata Bis 9 project (Grant number UMO-2019/34/E/NZ6/00137).

Author contributions

Conceptualisation, C.F.M., F.E.E., A.M.C and S.A.R.; Methodology, C.F.M., F.E.E., J.C.W., Y.X.H., T.K.P. , S.E., A.B., C.A.L., C.C.A., A.J.C., L.R.P., J.S.K., A.M.C and S.A.R.; Investigation, C.F.M., J.C.W., Y.X.H., T.K.P., B.J.M, K.A.B and C.C.R; Writing – Original Draft, C.F.M; Writing – Review & Editing, C.F.M., F.E.E., Y.X.H., T.K.P., A.B., C.A.L., C.C.A., A.J.C., L.R.P., J.S.K., A.M.C and S.A.R. Funding Acquisition, C.F.M., F.E.E., T.K.P., A.M.C and S.A.R.; Resources, J.S.K., T.K.P., A.M.C and S.A.R.; Supervision, A.M.C and S.A.R.

Declaration of interests

The authors declare no competing interests.

References

1. Welch, H. C. E. *et al.* P-Rex1 Regulates Neutrophil Function. *Curr. Biol.* **15**, 1867–1873 (2005).
2. Zhan, Y., Virbasius, J. V., Song, X., Pomerleau, D. P. & Zhou, G. W. The p40phox and p47phox PX Domains of NADPH Oxidase Target Cell Membranes via Direct and Indirect Recruitment by Phosphoinositides *. *J. Biol. Chem.* **277**, 4512–4518 (2002).
3. Schreiber, A. *et al.* Phosphoinositol 3-kinase-gamma mediates antineutrophil cytoplasmic autoantibody-induced glomerulonephritis. *Kidney Int.* **77**, 118–128 (2010).
4. Hoenderdos, K. *et al.* Hypoxia upregulates neutrophil degranulation and potential for tissue injury. *Thorax* **71**, 1030–1038 (2016).
5. Schlam, D. *et al.* Phosphoinositide 3-kinase enables phagocytosis of large particles by terminating actin assembly through Rac/Cdc42 GTPase-activating proteins. *Nat. Commun.* **6**, 8623 (2015).

6. Bohdanowicz, M., Cosío, G., Backer, J. M. & Grinstein, S. Class I and class III phosphoinositide 3-kinases are required for actin polymerization that propels phagosomes. *J. Cell Biol.* **191**, 999–1012 (2010).
7. Dewitt, S., Tian, W. & Hallett, M. B. Localised PtdIns(3,4,5)P3 or PtdIns(3,4)P2 at the phagocytic cup is required for both phagosome closure and Ca2+ signalling in HL60 neutrophils. *J. Cell Sci.* **119**, 443–451 (2006).
8. Marshall, J. G. *et al.* Restricted Accumulation of Phosphatidylinositol 3-Kinase Products in a Plasmalemmal Subdomain during Fcγ Receptor-Mediated Phagocytosis. *J. Cell Biol.* **153**, 1369–1380 (2001).
9. Dormann, D., Weijer, G., Dowler, S. & Weijer, C. J. In vivo analysis of 3-phosphoinositide dynamics during Dictyostelium phagocytosis and chemotaxis. *J. Cell Sci.* **117**, 6497–6509 (2004).
10. Giorgione, J. & Clarke, M. Heterogeneous modes of uptake for latex beads revealed through live cell imaging of phagocytes expressing a probe for phosphatidylinositol-(3,4,5)-trisphosphate and phosphatidylinositol-(3,4)-bisphosphate. *Cell Motil. Cytoskeleton* **65**, 721–733 (2008).
11. Servant, G. *et al.* Polarization of Chemoattractant Receptor Signaling During Neutrophil Chemotaxis. *Science* **287**, 1037–1040 (2000).
12. Yoo, S. K. *et al.* Differential Regulation of Protrusion and Polarity by PI(3)K during Neutrophil Motility in Live Zebrafish. *Dev. Cell* **18**, 226–236 (2010).
13. Wang, X. *et al.* Inhibitors of neutrophil recruitment identified using transgenic zebrafish to screen a natural product library. *Dis. Model. Mech.* **7**, 163–169 (2014).
14. Hellebrekers, P., Hietbrink, F., Vrisekoop, N., Leenen, L. P. H. & Koenderman, L. Neutrophil Functional Heterogeneity: Identification of Competitive Phagocytosis. *Front. Immunol.* **8**, 1498 (2017).

15. Levine, A. P., Duchen, M. R., Villiers, S. de, Rich, P. R. & Segal, A. W. Alkalinity of Neutrophil Phagocytic Vacuoles Is Modulated by HVCN1 and Has Consequences for Myeloperoxidase Activity. *PLOS ONE* **10**, e0125906 (2015).

16. Foote, J. R., Patel, A. A., Yona, S. & Segal, A. W. Variations in the Phagosomal Environment of Human Neutrophils and Mononuclear Phagocyte Subsets. *Front. Immunol.* **10**, 188 (2019).

17. Foote, J. R., Levine, A. P., Behe, P., Duchen, M. R. & Segal, A. W. Imaging the Neutrophil Phagosome and Cytoplasm Using a Ratiometric pH Indicator. *J. Vis. Exp. JoVE* 55107 (2017) doi:10.3791/55107.

18. Segal, A. W., Geisow, M., Garcia, R., Harper, A. & Miller, R. The respiratory burst of phagocytic cells is associated with a rise in vacuolar pH. *Nature* **290**, 406–409 (1981).

19. Jankowski, A., Scott, C. C. & Grinstein, S. Determinants of the phagosomal pH in neutrophils. *J. Biol. Chem.* **277**, 6059–6066 (2002).

20. Cech, P. & Lehrer, R. I. Phagolysosomal pH of Human Neutrophils. *Blood* **63**, 88–95 (1984).

21. Platkov, M., Tirosh, R., Kaufman, M., Zurgil, N. & Deutsch, M. Photobleaching of fluorescein as a probe for oxidative stress in single cells. *J. Photochem. Photobiol. B* **140**, 306–314 (2014).

22. Dolman, N. J., Kilgore, J. A. & Davidson, M. W. A Review of Reagents for Fluorescence Microscopy of Cellular Compartments and Structures, Part I: BacMam Labeling and Reagents for Vesicular Structures. *Curr. Protoc. Cytom.* **65**, 12.30.1-12.30.27 (2013).

23. Wood, A. J. T. *et al.* C5a impairs phagosomal maturation in the neutrophil through phosphoproteomic remodeling. *JCI Insight* **5**, e137029.

24. Prajsnar, T. K. *et al.* The autophagic response to Staphylococcus aureus provides an intracellular niche in neutrophils. *Autophagy* **17**, 888–902 (2021).

26. Pazhakh, V. *et al.* β-glucan–dependent shuttling of conidia from neutrophils to macrophages occurs during fungal infection establishment. *PLOS Biol.* **17**, e3000113 (2019).

27. Greene, C. J. *et al.* Macrophages disseminate pathogen associated molecular patterns through the direct extracellular release of the soluble content of their phagolysosomes. *Nat. Commun.* **13**, 3072 (2022).

28. Hawkins, P. T. & Stephens, L. R. PI3K signalling in inflammation. *Biochim. Biophys. Acta* **1851**, 882–897 (2015).

29. Sadhu, C., Masinovsky, B., Dick, K., Sowell, C. G. & Staunton, D. E. Essential role of phosphoinositide 3-kinase delta in neutrophil directional movement. *J. Immunol. Baltim. Md 1950* **170**, 2647–2654 (2003).

30. Elworthy, S. *et al.* Activated PI3K delta syndrome 1 mutations cause neutrophilia in zebrafish larvae. *Dis. Model. Mech.* **16**, dmm049841 (2023).

31. Lannutti, B. J. *et al.* CAL-101, a p110delta selective phosphatidylinositol-3-kinase inhibitor for the treatment of B-cell malignancies, inhibits PI3K signaling and cellular viability. *Blood* **117**, 591–594 (2011).

32. Camps, M. *et al.* Blockade of PI3Kgamma suppresses joint inflammation and damage in mouse models of rheumatoid arthritis. *Nat. Med.* **11**, 936–943 (2005).

33. Williams, O. *et al.* Discovery of dual inhibitors of the immune cell PI3Ks p110δ and p110γ: a prototype for new anti-inflammatory drugs. *Chem. Biol.* **17**, 123–134 (2010).

34. Gilbert, A. S. *et al.* Vomocytosis of live pathogens from macrophages is regulated by the atypical MAP kinase ERK5. *Sci. Adv.* **3**, e1700898 (2017).

35. Johnston, S. A. & May, R. C. The Human Fungal Pathogen Cryptococcus neoformans Escapes Macrophages by a Phagosome Emptying Mechanism That Is Inhibited by Arp2/3 Complex-Mediated Actin Polymerisation. *PLOS Pathog.* **6**, e1001041 (2010).

36. Bain, J. M. *et al.* Non-lytic expulsion/exocytosis of *Candida albicans* from macrophages. *Fungal Genet. Biol.* **49**, 677–678 (2012).

37. Quinn, S. E. *et al.* The structural dynamics of macropinosome formation and PI3-kinase-mediated sealing revealed by lattice light sheet microscopy. *Nat. Commun.* **12**, 4838 (2021).

38. Deladeriere, A. *et al.* The regulatory subunits of PI3Kγ control distinct neutrophil responses. *Sci. Signal.* **8**, ra8 (2015).

39. Suire, S. *et al.* Gbetagammas and the Ras binding domain of p110gamma are both important regulators of PI(3)Kgamma signalling in neutrophils. *Nat. Cell Biol.* **8**, 1303–1309 (2006).

40. Rathinaswamy, M. K. *et al.* HDX-MS-optimized approach to characterize nanobodies as tools for biochemical and structural studies of class IB phosphoinositide 3-kinases. *Structure* **29**, 1371-1381.e6 (2021).

41. Fey, P. D. *et al.* A genetic resource for rapid and comprehensive phenotype screening of nonessential Staphylococcus aureus genes. *mBio* **4**, e00537-00512 (2013).

42. Bernut, A. *et al.* Mycobacterium abscessus cording prevents phagocytosis and promotes abscess formation. *Proc. Natl. Acad. Sci. U. S. A.* **111**, E943-952 (2014).

43. Kwan, K. M. *et al.* The Tol2kit: a multisite gateway-based construction kit for Tol2 transposon transgenesis constructs. *Dev. Dyn. Off. Publ. Am. Assoc. Anat.* **236**, 3088–3099 (2007).

44. Prajsnar, T. K. *et al.* A privileged intraphagocyte niche is responsible for disseminated infection of Staphylococcus aureus in a zebrafish model. *Cell. Microbiol.* **14**, 1600–1619 (2012).

45. Salamaga, B. *et al.* Bacterial size matters: Multiple mechanisms controlling septum cleavage and diplococcus formation are critical for the virulence of the opportunistic pathogen Enterococcus faecalis. *PLOS Pathog.* **13**, e1006526 (2017).

Figures

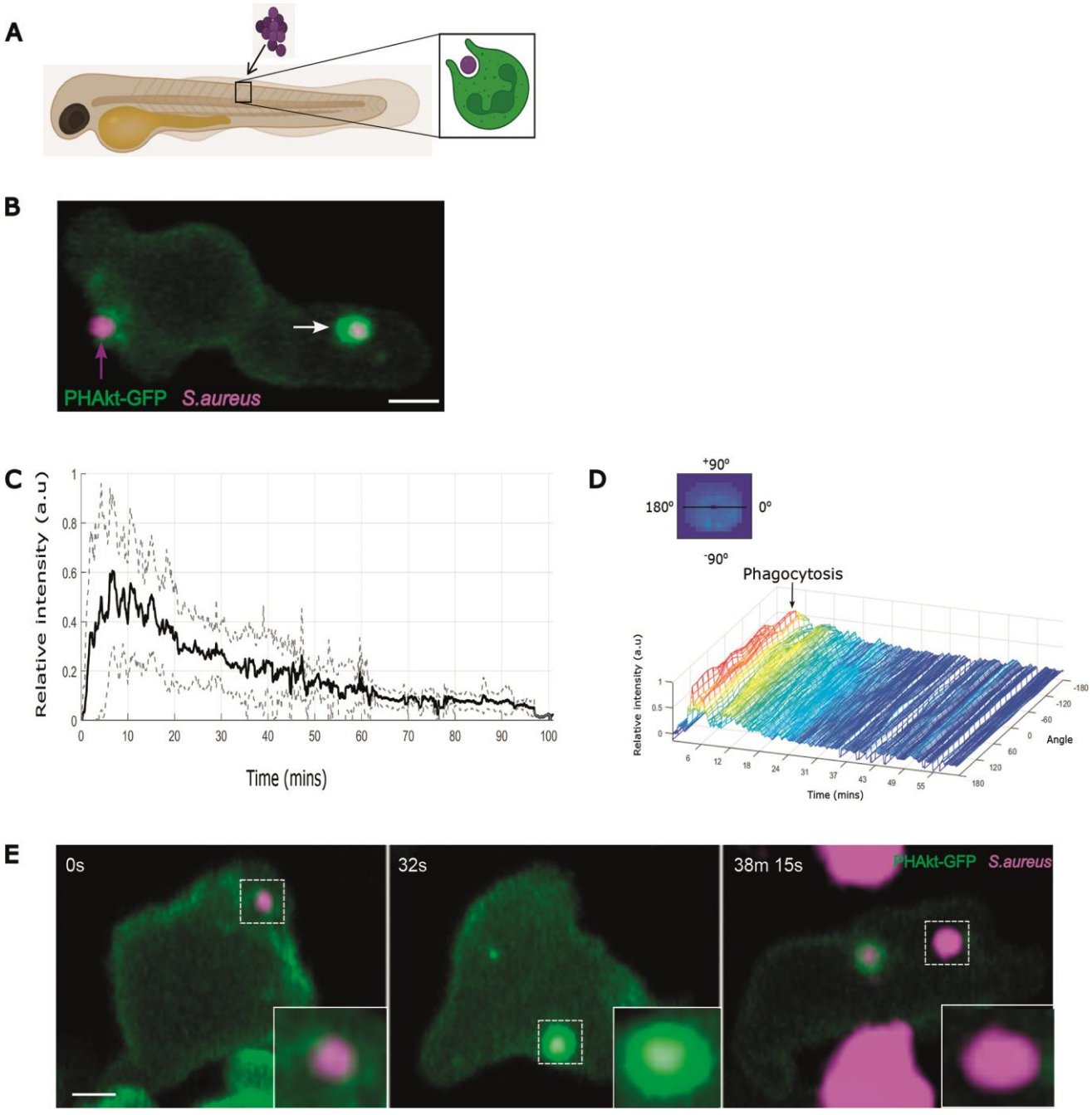

Fig. 1. Dynamics of PHAkt-eGFP on neutrophil phagosomes. (A) Schematic illustrating localised somite injection of *S.aureus* injection into day 3 *Tg(lyz:PHAkt-EGFP)i277* zebrafish larvae. **(B)** Image from a time-lapse capturing a neutrophil phagocytosing pHrodo™ Red *S.aureus* (magenta) (magenta arrow). Strong recruitment of PHAkt-eGFP (green) to the phagosome after cup closure

(white arrow). **(C)** Quantification of PHAkt-eGFP fluorescence on the phagosome membrane during phagocytosis of pHrodo™ Red *S.aureus*. Data shown is the average intensity values of 9 phagosomes from 4 independent larvae, from 4 experiments +/- SD. **(D)** Quantification of PHAkt-eGFP fluorescence to the phagosome membrane over time. **(E)** Sequential images illustrating PHAkt-eGFP recruitment to a neutrophil phagosome. Large clusters of strongly acidified bacteria are present within adjacent unlabelled, presumed macrophages. Scale Bar = 2µm.

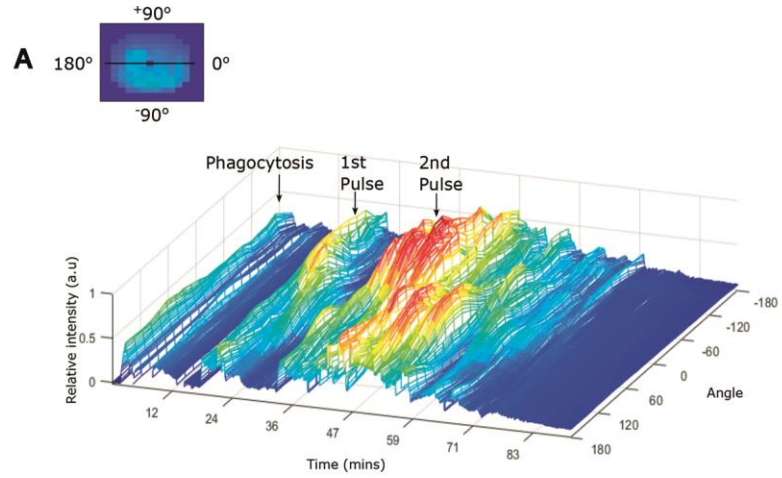

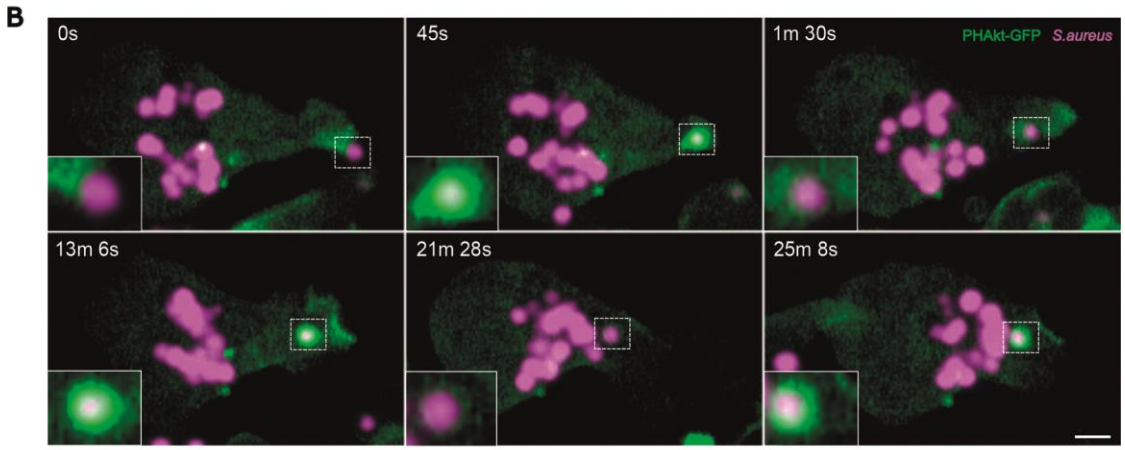

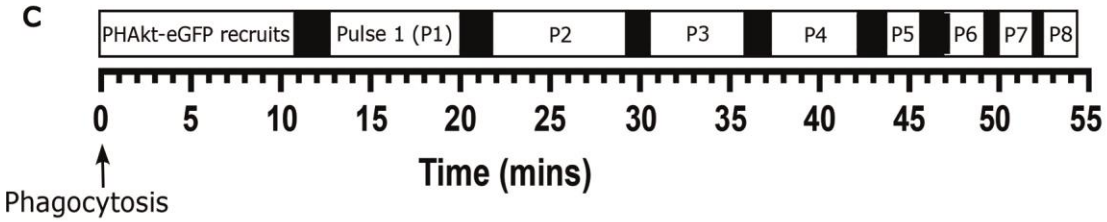

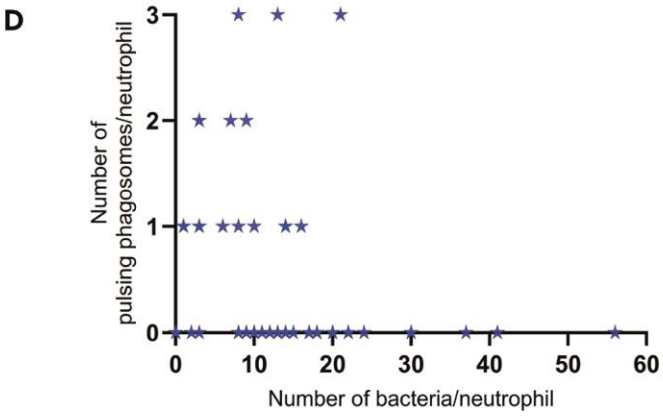

Fig.2. PHAkt-eGFP recruits in pulsatile bursts to neutrophil phagosomes. (A) Quantification of PHAkt-eGFP fluorescence on a pulsing phagosome. **(B)** Sequential images of a pulsing phagosome. 0s. Start of phagocytosis. 45s. Surge of PHAkt-eGFP recruitment as the phagosome closes. 1m30s. PHAkt-eGFP diminishes from the phagosome. 13m 6s. 1st pulse. 21m 28s. Loss of PHAkt-eGFP recruitment. 25m 8s 2nd pulse. Scale Bar = 2µm. **(C)** Schematic illustrating pulsatile recruitment of PHAkt-eGFP to phagosomes. Data represent average values from 152 phagosomes, from 11 independent larvae, from 11 experiments. **(D)** Pulses occur irrespective of the number of bacteria within a neutrophil. Data shown is from 55 neutrophils, from 11 independent larvae, from 11 experiments. Spearman's rank correlation between the number of bacteria inside neutrophils at time of 1st pulse or, for neutrophils with no pulsing phagosomes, after 30m of analysis and number of pulses/phagosome was -0.2733 with a corresponding p-value of 0.0415 (*).

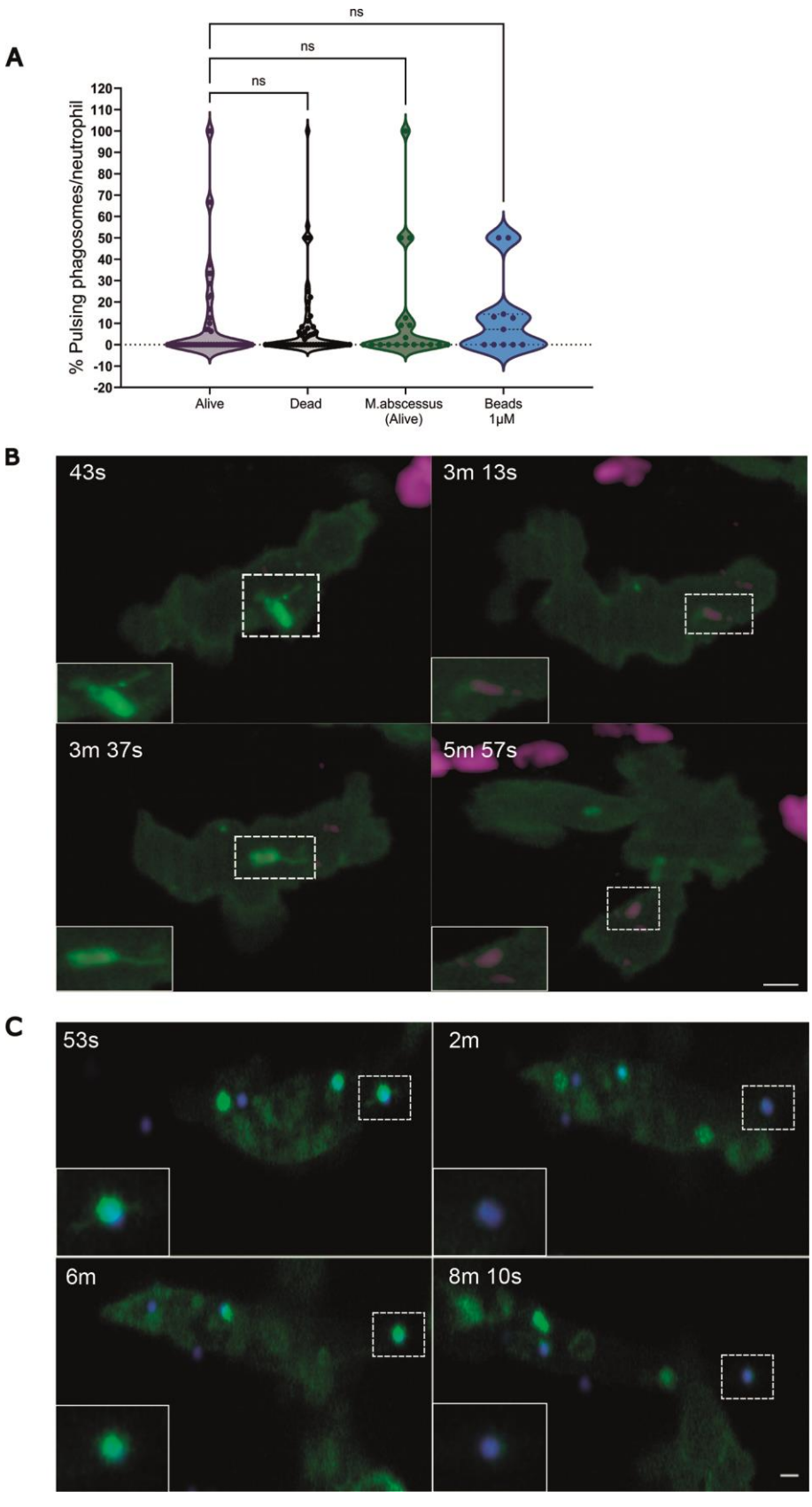

Fig. 3. Pulsatile bursts of PHAkt-eGFP recruitment are a neutrophil response to prey. (A) Violin plot showing the % of pulsing phagosomes per phagocytic neutrophil for live and dead *S.aureus*, live *M.abscessus* and 1µm beads. Data shown is the Median with the 25th and 75th percentiles. Live *S.aureus* = 46 phagosomes analysed from 11 independent larvae, from 11 experiments. Dead *S.aureus* = 54 phagosomes, 10 independent larvae, from 10 experiments. Live *M.abscessus* =18 phagosomes, 6 independent larvae, 6 experiments. 1µm beads= 11 phagosomes, 4 independent larvae, 4 experiments. **(B)** 'Pulses' occur on phagosomes containing *M.abscessus*. PHAkt-eGFP recruits to phagosomes during phagocytosis (43s) before gradually diminishing (3m 13s). PHAkt-eGFP then re-recruits to the phagosome ('1st pulse') (3m 37s) and then diminishes again (5m 57s). Scale Bar = 2µm. **(C)** 'Pulses' occur on phagosomes containing 1µm beads. PHAkt-eGFP recruits to phagosomes during phagocytosis 53s) before gradually diminishing (2m). PHAkt-eGFP then re-recruits to the phagosome ('1st pulse') (6m) and then diminishes again (8m 10s). Phagocytosis starts at 0mins. Scale Bar= 1µm.

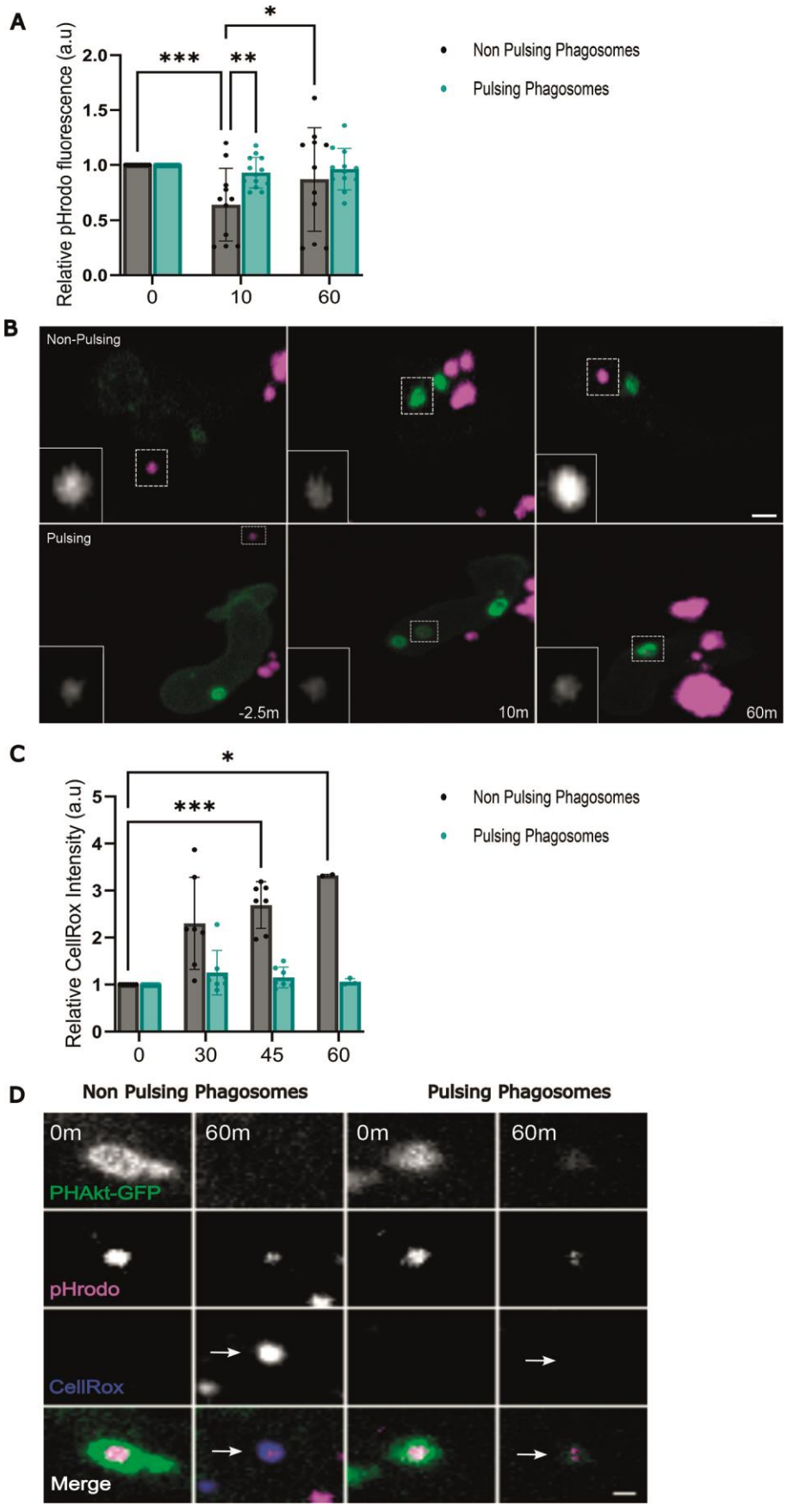

Fig. 4. pH change in pulsing phagosomes differs from non-pulsing phagosomes (A) Quantification of the relative change in fluorescence of pHrodo stained *S.aureus* on non-pulsing vs pulsing phagosomes. Data shown is the mean +/- SD. 0mins: 12 non-pulsing phagosomes, 14 pulsing phagosomes. 10mins: 11 non-pulsing phagosomes, 13 pulsing phagosomes. 60mins:11 non-pulsing phagosomes, 12 pulsing phagosomes, 11 independent larvae, 11 experiments. **(B)** Sequential timelapse images comparing the change in fluorescence of pHrodo stained *S.aureus* within pulsing vs non-pulsing phagosomes**.** Scale Bars = 2µm. **(C)** Quantification of the relative change in fluorescence of CellRox fluorescence within non-pulsing vs pulsing phagosomes. Data shown is the mean +/- SD. 0mins: 7 non-pulsing phagosomes, 7 pulsing phagosomes. 30mins: 7 non-pulsing phagosomes, 7 pulsing phagosomes. 45mins: 7 non-pulsing phagosomes, 7 pulsing phagosomes. 60mins. 2 non-pulsing phagosomes, 3 pulsing phagosomes, from 4 independent larvae, from 4 experiments. (**D)** Sequential images illustrating changes in CellRox fluorescence within non-pulsing vs pulsing phagosomes. Scale Bar = 1µm.

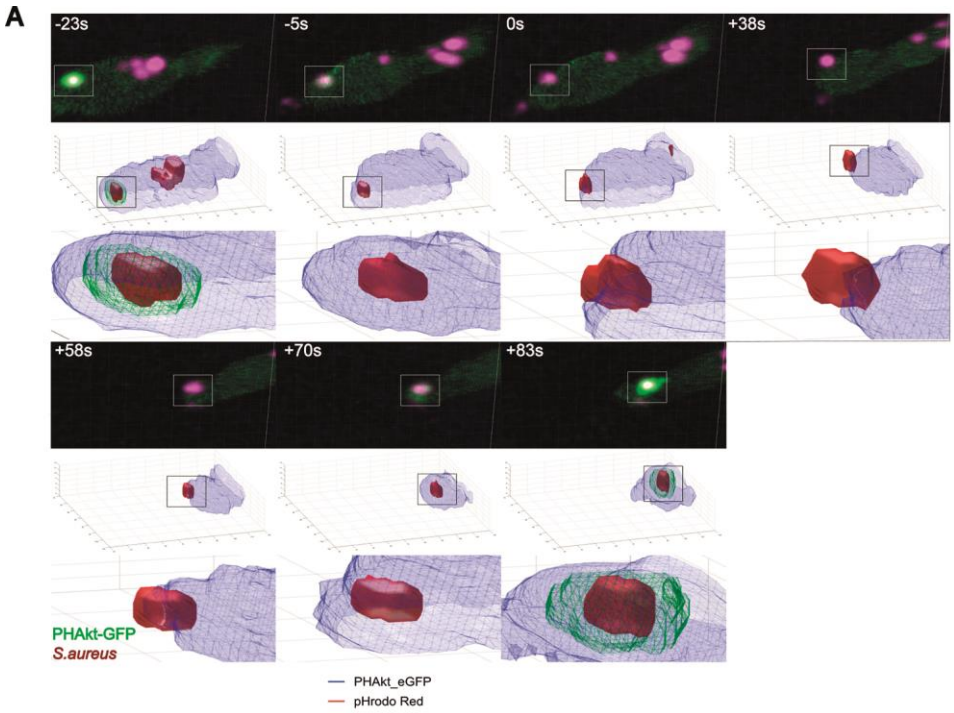

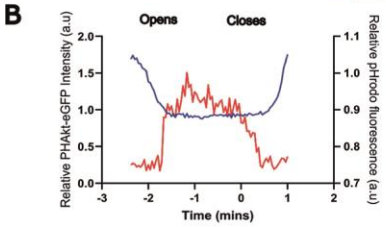

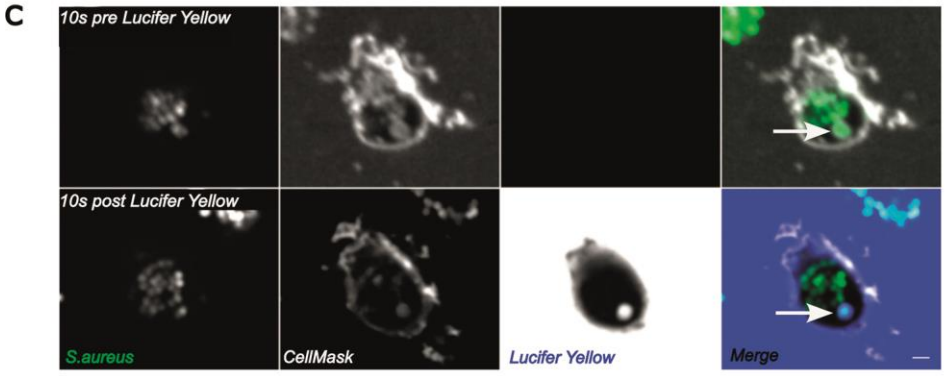

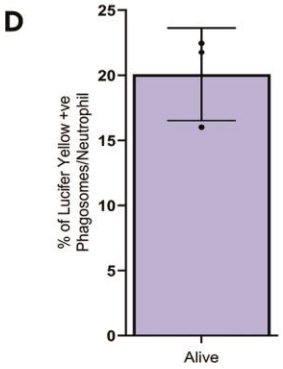

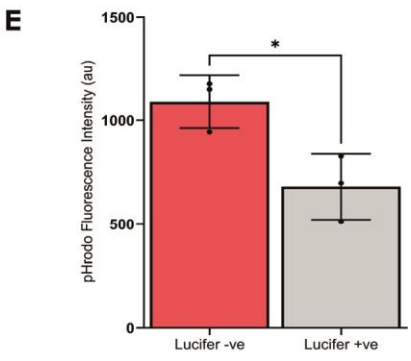

Fig. 5. A subset of neutrophil phagosomes may remain unsealed. (A) 3D reconstruction of PHAkt-eGFP dynamics when *S.aureus* is within a phagosome (-23s), the phagosome reopens (0s) and then recloses (+70s). **(B)** Quantification of the change in fluorescence of pHrodo stained *S.aureus* when a neutrophil phagosome reopens and closes. **(C)** Images illustrating the accumulation of Lucifer Yellow in a formed human neutrophil phagosome. There was a 20s delay between imaging, adding Lucifer yellow and then recommencing imaging as we needed to unload the plate from the microscope to add the dye. Scale Bar = 1µm. **(D)** Quantification of the % of Lucifer Yellow phagosomes in human neutrophils 30mpi. Data shown is the mean +/- SD. 2779 phagosomes analysed from 3 experiments. **(E)** Quantification of pHrodo fluorescence in Lucifer Yellow -ve vs Lucifer Yellow +ve phagosomes 60mpi. Data shown is the mean +/- SD. 4369 phagosomes analysed from 3 experiments.

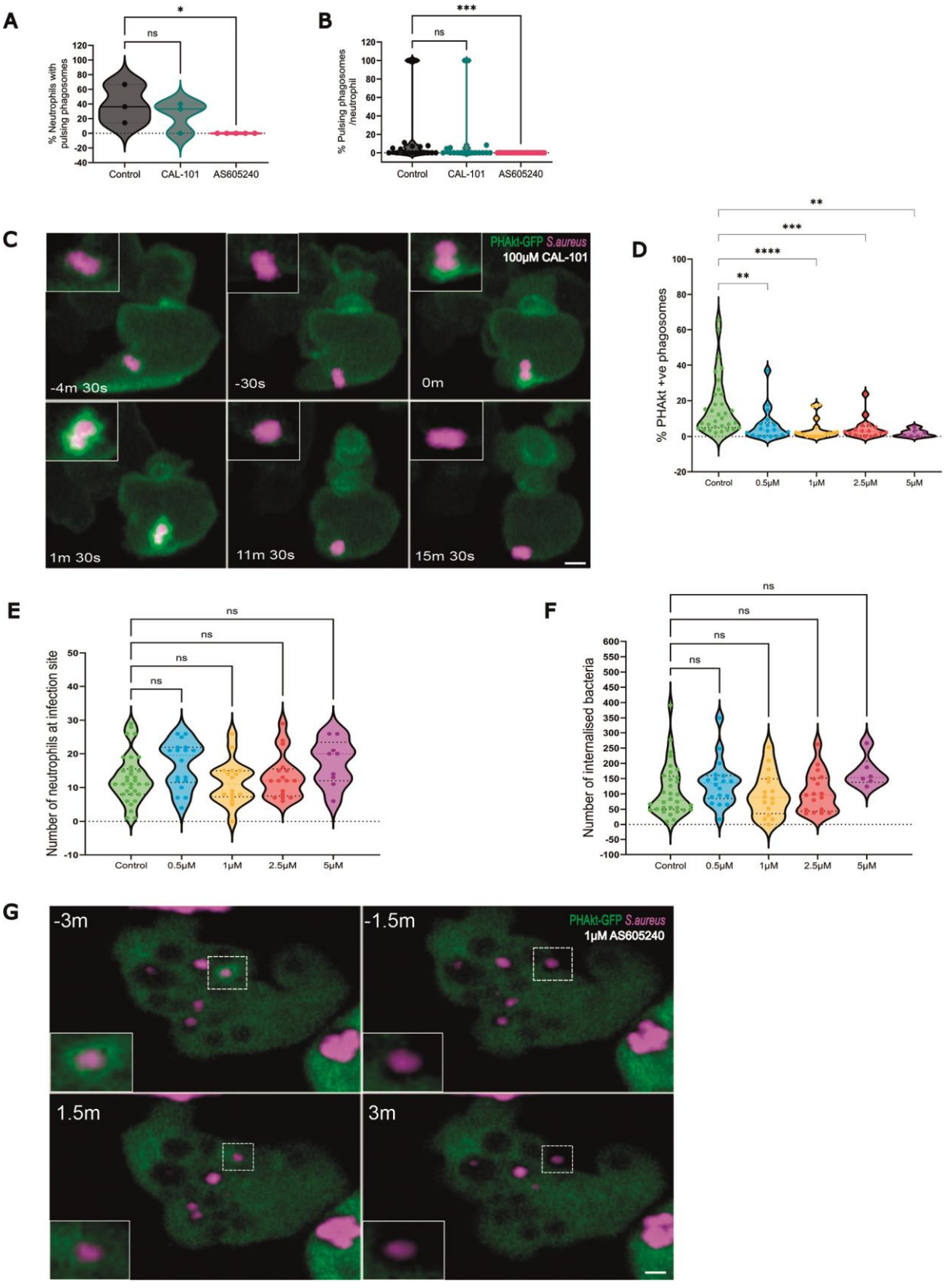

Fig. 6. Pulses of PHAkt occur despite inhibition with CAL-101 and are abolished by AS605240. **(A)** Violin plot showing the % of neutrophils that have pulsing phagosomes. Timelapse started 2hours post infection following 30min incubation of *Tg(lyz:PHAkt-EGFP)i277* larvae with 100µm CAL-101 and 1µm AS605240. Data shown is the Median with the 25th and 75th percentiles from 87 neutrophils, 11 independent larvae, 11 experiments. **(B)** Violin plot showing % of pulsing phagosomes in each neutrophil in a timelapse starting 2hours post infection following 30min incubation of *Tg(lyz:PHAkt-eGFP)i277* larvae with 100µm CAL-101 and 1µm AS605240. Data shown is the Median with the 25th and 75th percentiles from 780 phagosomes, 11 independent larvae, 11 experiments. **(C)** Sequential images illustrating pulsatile recruitment of PHAkt-eGFP to a phagosome exposed to 100µm CAL-101. Scale Bar = 2µm. **(D)** Violin plot showing quantification of the % of PHAkt-eGFP +ve phagosomes 2 hours post infection following 30mins incubation with AS605240. Data shown is the median with the 25th and 75th percentiles from 6 independent larvae, from 6 experiments. **(E)** Violin plot showing quantification of the number of neutrophils at a *S.aureus* infection site 2hours post infection following 30mins incubation with AS605240. Data shown is the median with the 25th and 75th percentiles from 6 independent larvae, 6 experiments. **(F)** Violin plot showing quantification of the number of bacteria/neutrophil 2hours post infection following 30mins incubation with AS605240. Data shown is the median with the 25th and 75th percentiles from 6 independent larvae from 6 independent larvae, from 6 experiments. **(G)** Sequential images illustrating that PHAkt-eGFP recruits to neutrophil phagosomes prior to exposure to 1µm AS605240 (3m before attempted rephagocytosis (-3m). Bacteria is then released from the phagosome (-1.5m). Following exposure to 1µm AS605240, the neutrophil attempts to rephagocytose the bacteria but PHAkt-eGFP does not recruit to the phagosome (1.5m) and the bacteria is released from the phagosome (3m). Scale Bar = 2µm.

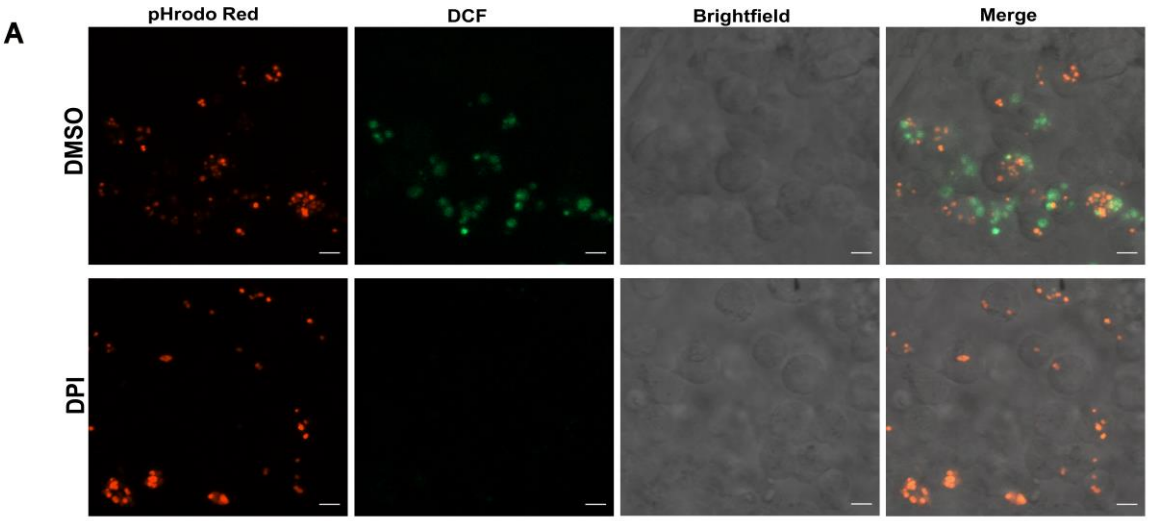

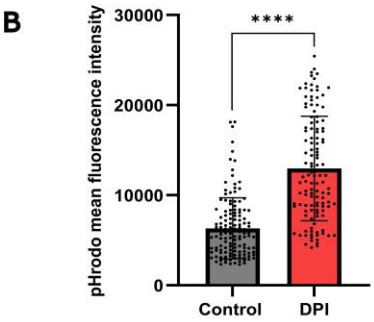

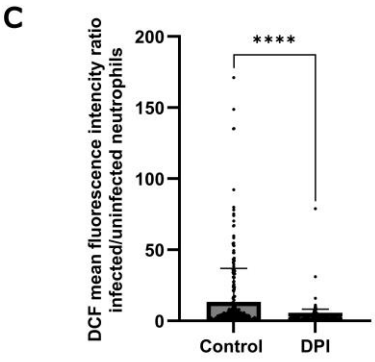

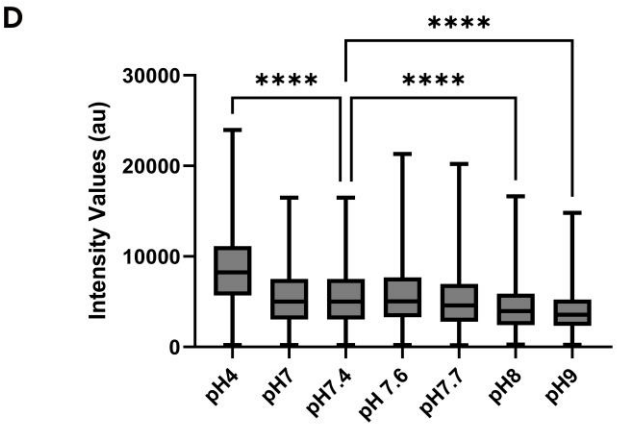

Fig. S1. NADPH oxidase drives the alkalinisation of the neutrophil phagosome. (A) Confocal images illustrating that the fluorescence of pHrodo Red-labelled internalised bacteria is higher and that the fluorescence of the ROS detector, DCF, dims when NADPH oxidase is inhibited in zebrafish larvae. **(B)** Quantification of the fluorescence of pHrodoRed stained *S.aureus* in control (DMSO) and NADPH oxidase-inhibited (DPI) zebrafish larvae, 11 larvae analysed from 2 independent experiments. Number of internalised bacterial clusters analysed: DMSO – 281, DPI – 251. **(C)** Quantification of the fluorescence of the ROS detector, DCF, in control (DMSO) and NADPH oxidase inhibited (DPI) zebrafish larvae, 11 larvae analysed from 2 independent experiments. Number of internalised bacterial clusters analysed: DMSO: 281, DPI: 251. **(D)** Quantification of the fluorescence of pHrodo Red stained *S.aureus* in different pH PBS solutions.

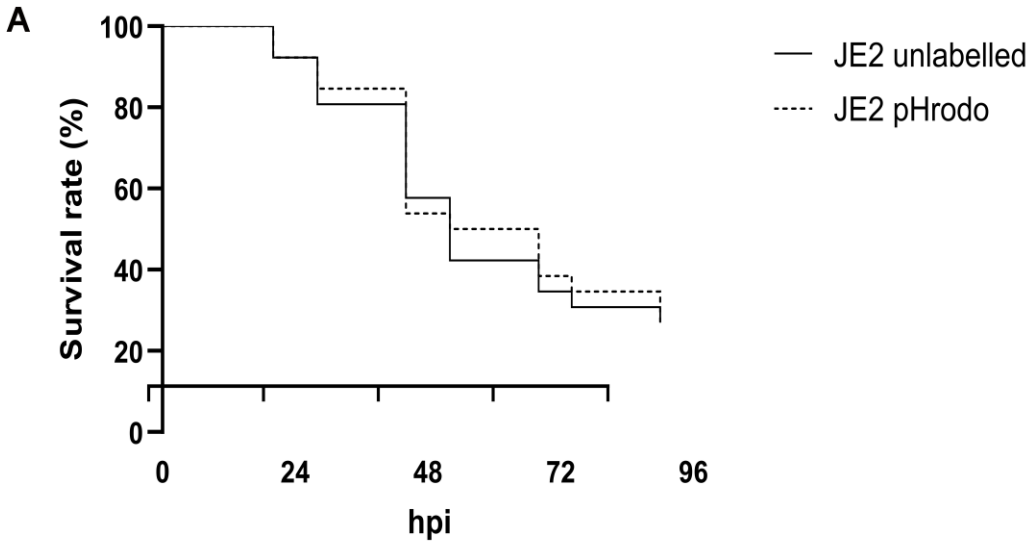

Fig. S2. (A) pHrodo staining does not alter the pathogenicity of *S.aureus*. 52 larvae analysed from 1 experiment.

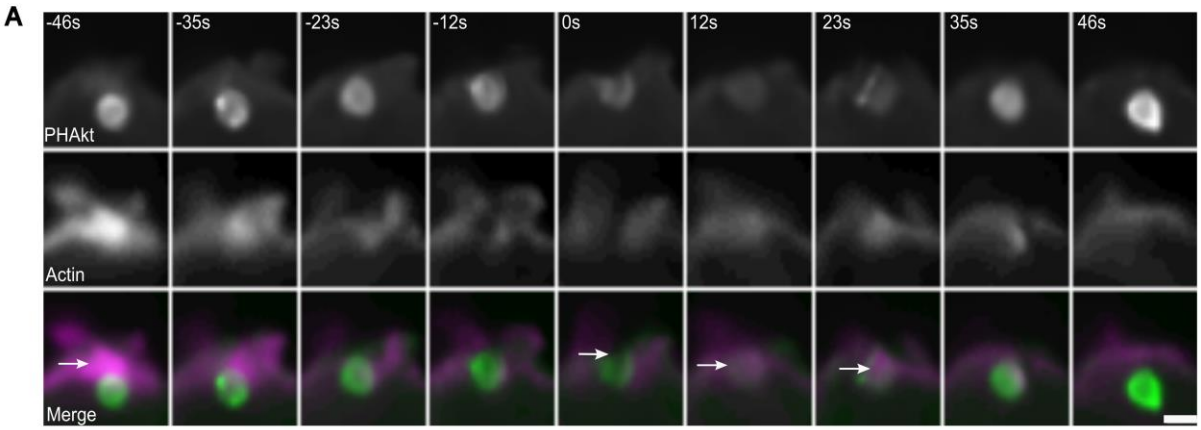

Fig. S3. Sequential images capturing the dynamics of PHAkt-eGFP and actin when bacteria are released and recaptured from a phagosome. Cortical actin fibres are visualised overlying the phagosome at 46s (arrow). At 0s, arrow shows the separation of cortical actin filaments as pulsing phagosome reopens onto the neutrophil surface. At 23s, actin filaments shape the phagocytic cup and surround the phagosome (arrow). Scale Bar = 2µm.

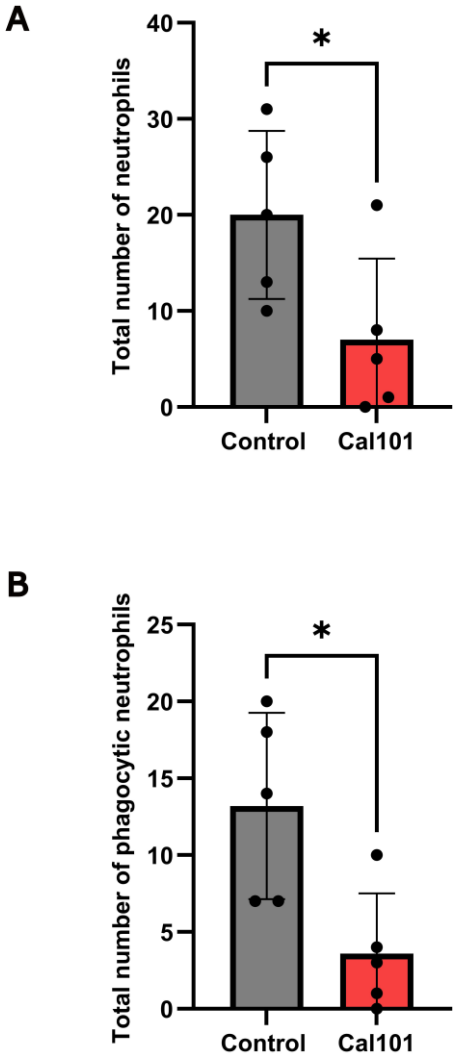

Fig. S4. CAL-101 reduces the number of neutrophils recruited to an *S.aureus* infection site. **(A)** Quantification of the number of neutrophils at an *S.aureus* infection site 2 hours post-infection following 30mins incubation with 100µm of CAL-101. Data shown is the mean +/- SD from 5 independent larvae, 5 experiments. **(B)** Quantification of the number of phagocytic neutrophils at a *S.aureus* infection site 2 hours post-infection following 30mins incubation with 100µm of CAL-101. Data shown is the mean +/- SD from 5 independent larvae, 5 experiments.

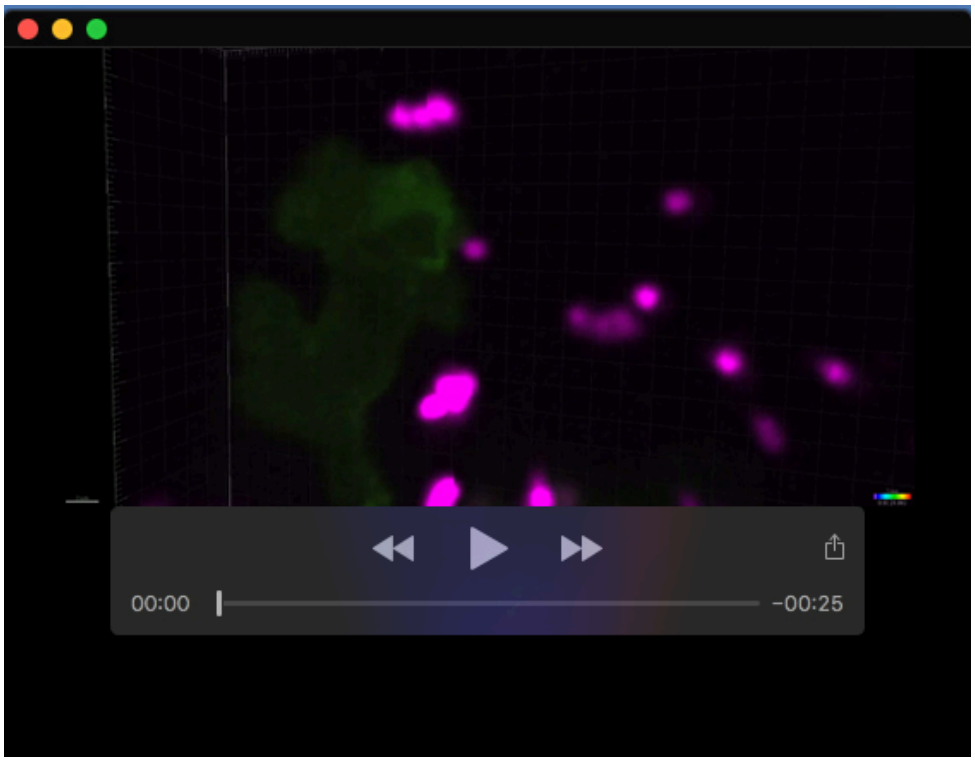

Movie 1. Dynamics of PHAkt-eGFP on neutrophil phagosomes following infection with *S.aureus*. Minimal PHAkt-eGFP recruits during early formation of the phagocytic cup. PHAkt-eGFP recruits strongly at sites of cup closure (white arrows) and uniformly to the phagosome membrane after cup formation (white arrows). Green = PHAkt-eGFP. Magenta = pHrodo™ Red stained *S.aureus*.

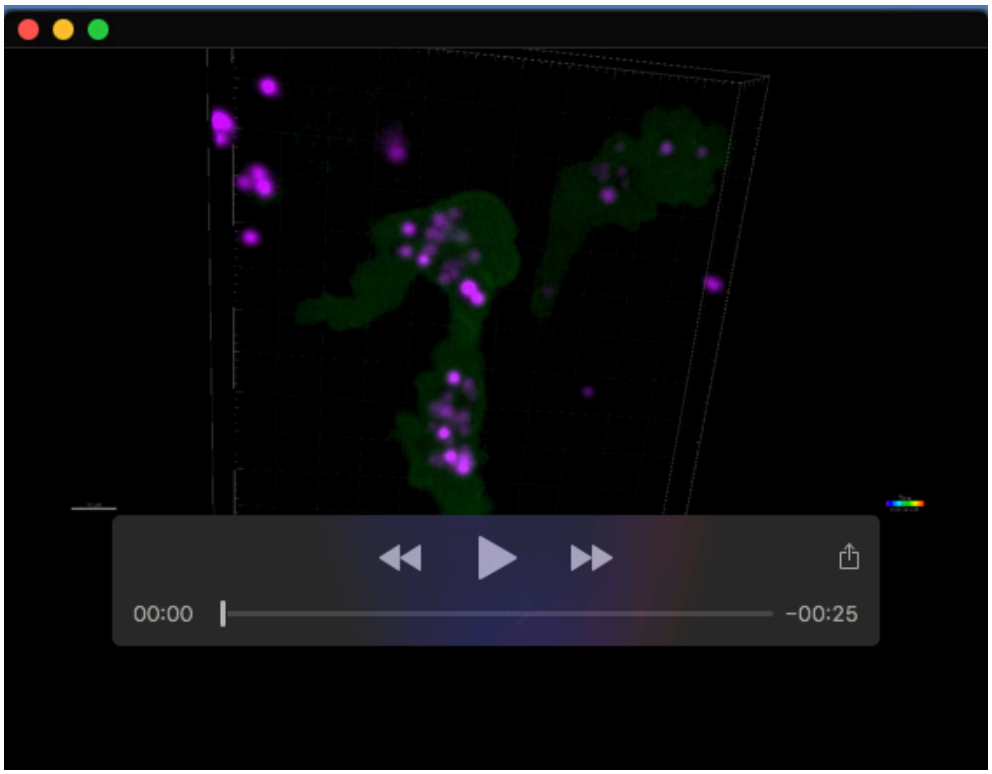

Movie 2. Pulsatile recruitment of PHAkt-eGFP to a neutrophil phagosome containing *S.aureus*. Green = PHAkt-eGFP. Magenta = pHrodo™ Red stained *S.aureus*.

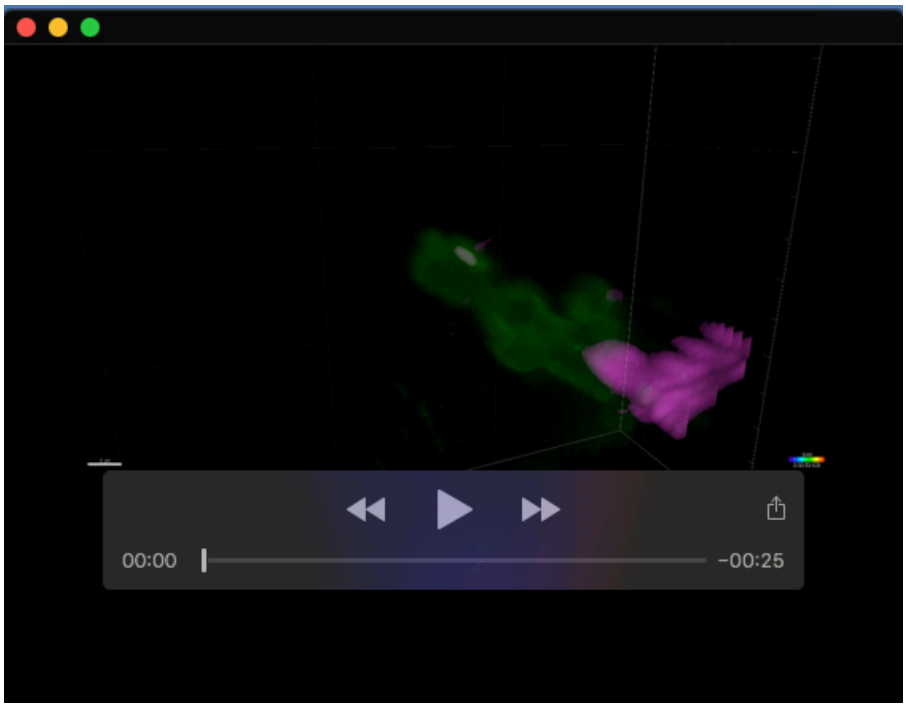

Movie 3. Pulsatile recruitment of PHAkt-eGFP to a neutrophil phagosome containing *Mycobacterium abscessus*. Green = PHAkt-eGFP. Magenta = pHrodo™ Red stained *M.abscessus*.

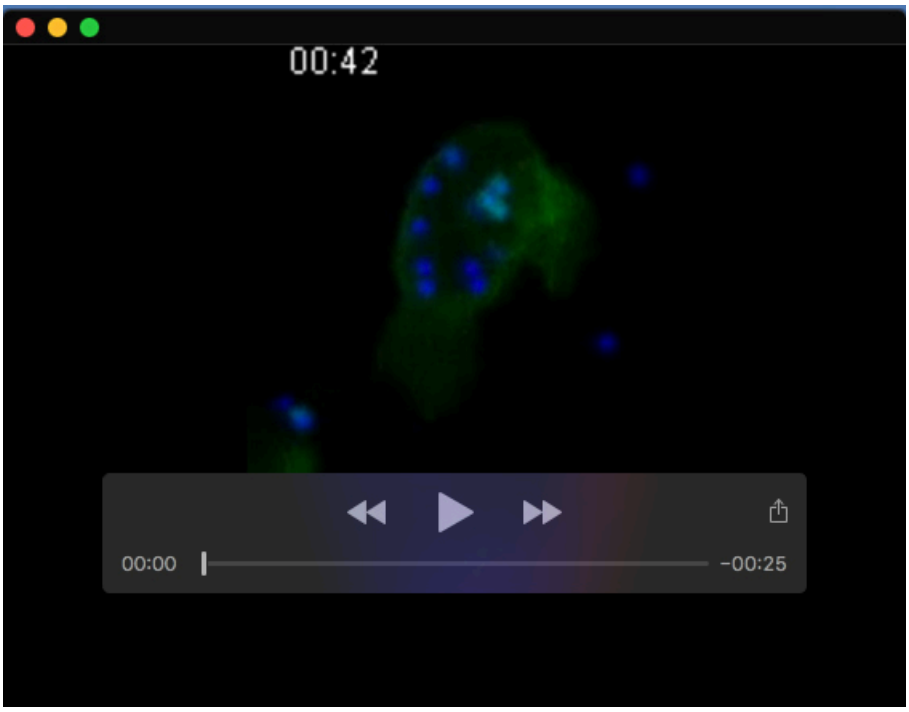

Movie 4. Pulsatile recruitment of PHAkt-eGFP to a neutrophil phagosome containing 1µm latex beads (blue spheres). 1µm bead is within the neutrophil at the start of the movie. PHAkt-eGFP recruits to the phagosome membrane (3m 5s) (Pulse). PHAkt-eGFP then dissipates from the phagosome membrane (8m 34). Green = PHAkt-eGFP. 1µm latex beads (blue spheres).

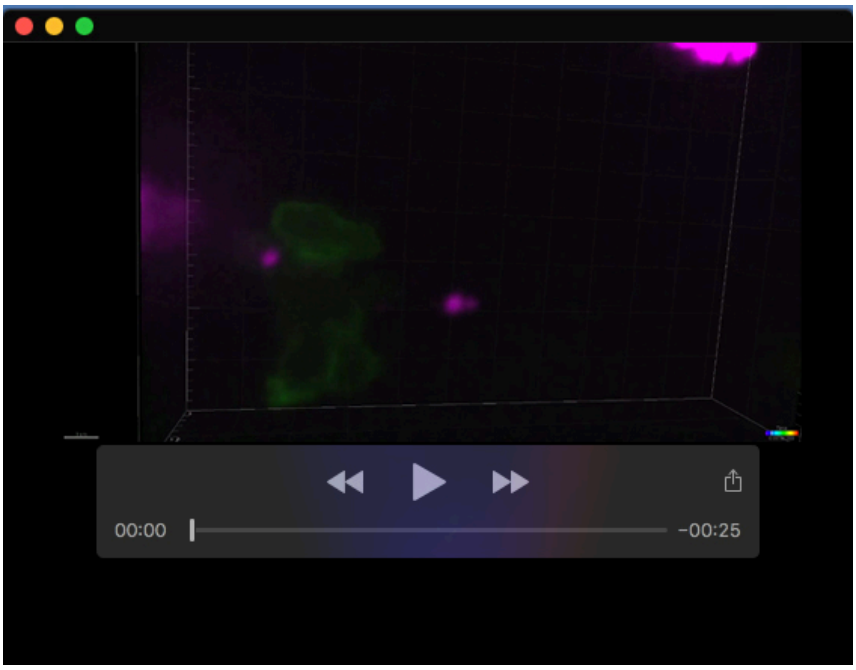

Movie 5. Neutrophil expelling and recapturing *S.aureus*. A neutrophil phagocytoses *S.aureus* (12s). PHAkt-eGFP (green) identifies the plasma and phagosome membranes. *S.aureus* is expelled from the phagosome onto the surface of the neutrophil (29s). *S.aureus* is recaptured by the neutrophil (1st pulse) (33s). Green = PHAkt-eGFP. Magenta = pHrodo™ red stained *S.aureus*.

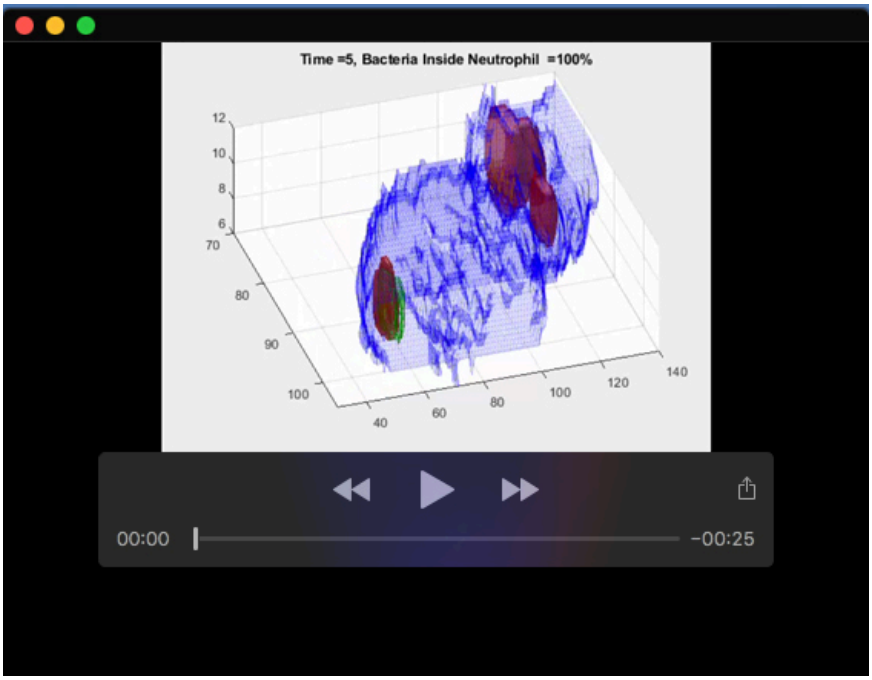

Movie 6. 3D reconstruction of a pulsing phagosome showing that a neutrophil phagosome reopens and recloses. *S.aureus* is within a phagosome at the start of the movie. PHAkt-eGFP recruits to the phagosome. PHAkt-eGFP diminishes from the phagosome membrane and *S.aureus* is released from the phagosome onto the surface of the neutrophil. *S.aureus* is recaptured by the neutrophil and PHAkt-eGFP re-recruits to the phagosome membrane (1st pulse). Yellow cage shows the % of the bacteria which is expelled from the phagosome. Green = PHAkt-eGFP. Red = pHrodo™ red stained *S.aureus*.

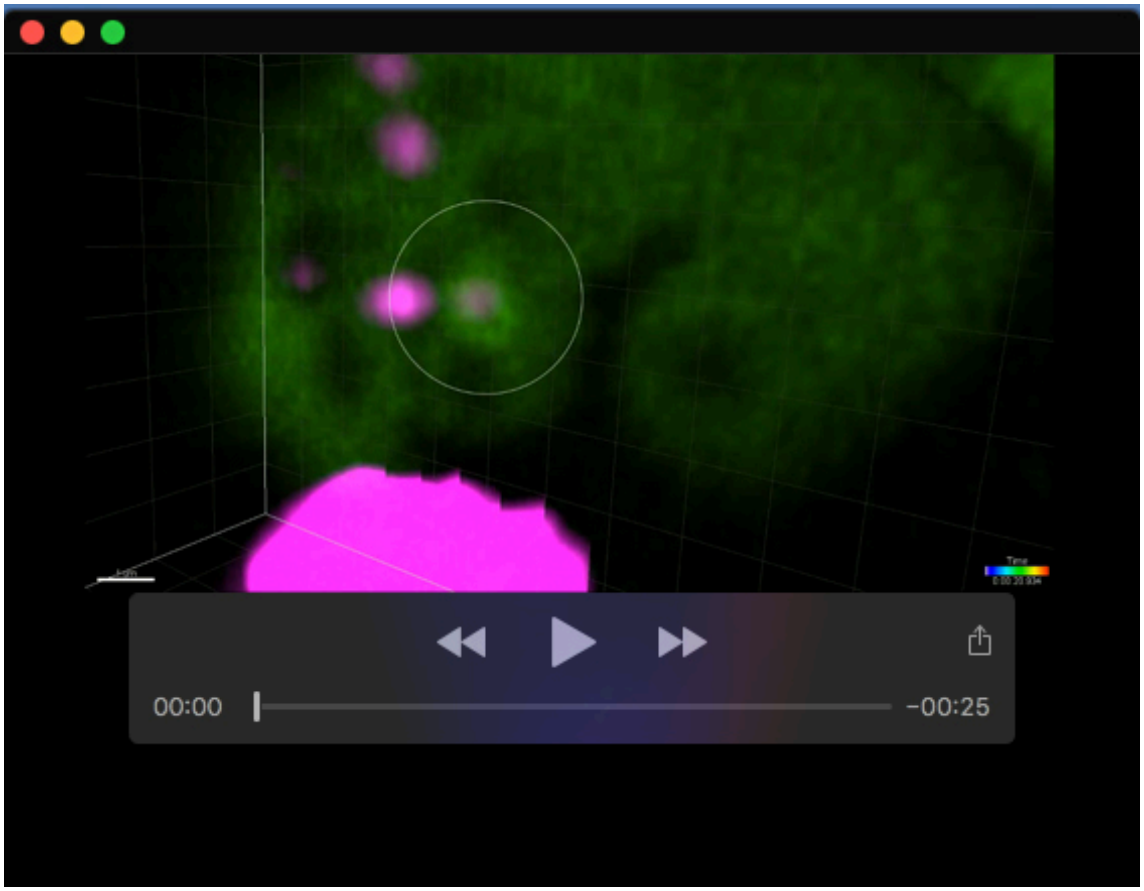

Movie 7. PI3Kγ inhibition prevents pulsatile recruitment of PHAkt-eGFP to neutrophil phagosomes. *S.aureus* is within a phagosome at the start of the movie (white circle). *S.aureus* is then released from the phagosome (28s). Neutrophil then attempts to rephagocytose *S.aureus* (1m 43s) (blue dot) but PHAkt-eGFP does not re-recruit (pulse) to the phagosome. Green = PHAkt-eGFP. Magenta = pHrodo™ Red stained *S.aureus*.